Title:

A single fungal MAP kinase controls plant cell-to-cell invasion by the rice blast fungus

Authors: Wasin Sakulkoo[1], Miriam Osés-Ruiz[1], Ely Oliviera Garcia[2], Darren M. Soanes[1], George R. Littlejohn[1†], Christian Hacker[1], Ana Correia[1], Barbara Valent[2], Nicholas J. Talbot[1*]

Affiliations:

[1]School of Biosciences, University of Exeter, Exeter, EX4 4QD, United Kingdom.

[2]Department of Plant Pathology, Kansas State University, 4024 Throckmorton Plant Sciences Center, Manhattan, KS 66506-5502, USA

[†]Present Address: School of Biological and Marine Sciences, Plymouth University, Portland Square Building, Drake Circus, Plymouth, PL4 8AA, UK

[*]Corresponding to: Nicholas J. Talbot N.J.Talbot@exeter.ac.uk

Abstract:

Blast disease destroys up to 30% of the rice crop annually and threatens global food security. The blast fungus *Magnaporthe oryzae* invades plant tissue with hyphae that proliferate and grow from cell to cell, often through pit fields where plasmodesmata cluster. Here we show that chemical genetic inhibition of a single fungal MAP kinase, Pmk1, prevents *M. oryzae* from infecting adjacent plant cells, leaving the fungus trapped within a single plant cell. Pmk1 regulates expression of secreted fungal effector proteins implicated in suppression of host immune defenses, preventing reactive oxygen species generation and excessive callose deposition at plasmodesmata. Furthermore, Pmk1 controls constriction of hyphae required for fungal growth from one rice cell to the neighboring cell, enabling host tissue colonization and blast disease.

One sentence summary:

A fungal MAP-kinase controls hyphal diameter and suppresses host defenses as the fungus grows through intercellular channels.

Word Count: 2923 words

(3123 total words, including 22 refs for main manuscript. Allowing reduction of 200 words for titles in print version)

Main text:

Blast diseases of cereals are caused by the filamentous fungus *Magnaporthe oryzae* (synonym of *Pyricularia oryzae*), destroying sufficient rice each year to feed 60 million people (*1*), while wheat blast disease now threatens wheat production in South America and, most recently, Asia (*2*). Plant infection requires an infection cell, called an appressorium, which uses a pressure-driven mechanism to breach the tough cuticle of the leaf (*3, 4*). Once inside plant tissue, the fungus elaborates pseudohypha-like invasive hyphae which rapidly colonize living host cells, secreting effector molecules to suppress host immunity and facilitate infection (*5*). *M. oryzae* effectors are delivered into host cytoplasm by means of a biotrophic interfacial complex (BIC), a plant-derived membrane-rich structure in which effectors accumulate during transit to the host (*5-8*). Hyphae then appear to locate pit fields, composed of plasmodesmata, which are traversed by constricted, narrow hyphae enabling spread of the fungus to adjacent host cells (*9*). The fungus rapidly colonizes host tissue and disease lesions appear within 4-5 days of initial infection by spores.

In this study, we set out to investigate how *M. oryzae* colonizes host tissue and, in particular, how it spreads from one plant cell to the next. We first performed ultrastructural analysis of rice sheath cells infected by pathogenic strain Guy11. This confirmed constriction of hyphae from an average diameter of 5.0 μm to 0.6 μm while traversing rice cells (Fig. 1, A and B; fig. S1). The rice plasma membrane in the second invaded cell remained intact as an electron-dense lining near the rice cell wall, continuous with plant plasma membrane around hyphae (Fig. 1B) (*5, 8, 9*). By contrast, the rice plasma membrane in the first-invaded cell lost integrity upon exit of the fungus to the next rice cell (Fig. 1B and E) (*7, 9, 10*).

One of the plant's defenses against infection is to close intercellular plasmodesmata channels by deposition of callose (*11, 12*). We visualized callose using aniline blue staining of rice cells (Fig. 1C; fig. S3). Callose papillae often form at appressorium penetration sites, but no callose occlusions are initially observed at plasmodesmata during infection of the first rice cell at 27h (fig. S3). Later callose deposition is observed at plasmodesmata by 30h, consistent with the onset of cell death of initially invaded rice cells (fig. S1, figS2). Callose collars then form around the base of invasive hyphae after they invade adjacent cells, 34h following infection (Fig. 1C; fig. S3). These observations suggest *M. oryzae* is able to clear plasmodesmatal occlusion materials before penetrating pit fields (Fig. 1D). We also observed a switch from polarized to isotropic fungal growth by invasive hyphae at rice cell junctions. A polarisome marker Spa2-GFP localizes to hyphal tips and then disappears as hyphal tips swell upon contact with the host cell wall (fig. S2) (*5*). Spa2-GFP then appears again at hyphal tips in newly colonized cells (fig. S2). Cell wall crossing is accompanied by re-organisation of fungal septins and F-actin into an hourglass shape at the point of maximum hyphal constriction (Fig. 1F; fig. S2 and S10; movie S1) (*3, 5, 13*).

Plasmodesmata are dynamic structures through which proteins diffuse between plant cells (*11*). To test whether the blast fungus can manipulate plasmodesmata by increasing their size exclusion limit, to facilitate effector diffusion to adjacent plant cells, we bombarded rice tissue infected with *M. oryzae* at 24h post inoculation (hpi) using single and double-sized mCherry expression vectors. In uninfected rice tissue, we observed that a 28.8-kDa single mCherry protein moves into neighboring rice cells, but a 57.6-kDa double mCherry fusion protein generally does not, due to its larger size (Fig. 1 G and H). By contrast, in blast-infected tissue, double mCherry protein diffused to adjacent rice cells. The gating limit of rice plasmodesmata is therefore relaxed during early *M. oryzae* infection. We then carried out time-lapse imaging of the fungal apoplastic effector Bas4-GFP (Biotrophy-associated secreted protein 4) (*8*) during plant infection, expressed under its native promoter (fig. S2; movie S2). We observed that upon exit of the fungus to an adjacent cell, Bas4-GFP leaked into host cytoplasm of initially colonized rice cells. However, fluorescence did not diffuse into the newly colonized cells. Plasmodesmata therefore remain open at early stages of infection (24-27 hpi), but closed at later stages, consistent with the increase in plasmodesmatal callose deposition at 30-34 hpi (fig. S3) (*7, 14*), suggesting that the blast fungus is able to overcome callose deposition at pit fields to invade neighboring cells. Plasmodesmata may lose their structural integrity after this time, as initially infected rice cells lose their viability.

To study regulatory mechanisms controlling invasive growth, we characterized Pmk1, a fungal mitogen-activated protein kinase (MAPK) essential for appressorium development and pathogenicity, that is conserved in many plant pathogenic fungi (*15*). Pmk1 null mutants *M. oryzae* cannot infect rice plants even when mutants are inoculated on wounded leaves (*15*). We decided to conditionally inactivate the Pmk1 MAPK, using a chemical genetic approach. We generated an analogue-sensitive (AS) allele of *PMK1* (*pmk1*^{AS}) by mutating the gatekeeper residue of the kinase ATP-binding site into a small amino acid residue, glycine. The equivalent (Shokat) mutation previously reported in yeast *fus3-as1* confers susceptibility to an ATP analogue 1-Naphthyl-PP1 (1NA-PP1) (*16*). Expression of the *pmk1*^{AS} allele, under control of its native promoter, restores pathogenicity to a Δ*pmk1* mutant (fig. S4). Addition of 1NA-PP1 selectively inhibited the function of Pmk1^{AS} mutants, preventing appressorium development (fig. S4), identical to the effects of *PMK1* deletion or expression of a kinase inactive allele (*17*). We also observed that inhibiting Pmk1 after appressorium formation blocked cuticle penetration by preventing assembly of the septin ring at the appressorium pore (fig. S5).

To test the role of Pmk1 in tissue invasion, we allowed a *pmk1*^{AS} mutant to invade the first rice epidermal cell before adding 1NA-PP1 at 26 hpi. This treatment blocked invasion of adjacent epidermal cells, resulting in the first-infected cells becoming filled with fungal hyphae (Fig. 2, A and B). Pmk1 inactivation did not impact the structure of BICs, or affect morphology of invasive hyphae (fig. S6A). In the presence of 1NA-PP1, hyphae of the *pmk1*^{AS} mutant still form terminal swellings at host wall contact points (Fig. 2C) (*9*) but cannot breach adjacent cells. Inhibition of Pmk1 also blocked rice cell invasion in a second rice

cultivar, Mokoto, and barley (fig. S6, B and C). Pmk1 inhibition was accompanied by rapid de-repression of reactive oxygen species (ROS) generation, a key plant defense response, and increased ROS-dependent callose deposition (Fig. 2, D and E; fig. S6). To confirm the role of Pmk1 in cell wall crossing, we performed live-cell imaging of a functional Pmk1-GFP protein, which showed its expression during appressorium-dependent cuticle penetration (Fig. 2F) (*17*), but also when invasive hyphae contact rice cell walls, just prior to invasion of the neighboring cell (Fig. 2G; movie S4). *M. oryzae* possesses two additional MAPKs, Osm1 which is dispensable for virulence (*18*), and Mps1 which regulates cell integrity and is necessary for fungal infection (*19*). We therefore generated a *mps1*^{AS} mutant and found that selective inactivation of Mps1 enhanced host defenses (*20*), but did not block cell-to-cell invasion (fig. S7).

To investigate how Pmk1 regulates invasive growth, we performed RNA-seq analysis to compare *M. oryzae* gene expression during infection by the *pmk1*^{AS} mutant in the presence or absence of 1NA-PP1. Using an adjusted *P*-value ≤ 0.05 for differential gene expression, 1,457 fungal genes were altered in expression during Pmk1 inhibition, accounting for 11.5 % of total protein encoding genes. Of these, 715 fungal genes were up-regulated and 742 fungal genes down-regulated (Table S2). A subset of effector genes implicated in plant immunity suppression were positively regulated by Pmk1, including AVR-Pita1 (*6*), Slp1, which suppresses chitin-triggered immunity (*21*), Avr-Pik, and several Bas effectors, including Bas2 and Bas3 effectors (*8*) that putatively function at cell wall crossing sites (Fig. 3A; fig S8). We expressed Bas2-GFP and Bas3-GFP in the *pmk1*^{AS} mutant and found they were not expressed in the presence of 1NA-PP1 (Fig. 3B and C). We also generated a *pmk1*^{AS} strain expressing cytosolic GFP under control of the Bas3 promoter (Fig 3D-F). Addition of 1NA-PP1 inhibited GFP expression during appressorium-mediated infection (Fig 3D) and during invasive growth (Fig E, F). Localization of other fungal effectors was not affected by Pmk1 inactivation (fig. S8) and Pmk1 therefore affects expression of a subset of fungal effectors involved in suppression of host immunity.

To test whether suppression of host immunity, particularly at plasmodesmata, could explain the role of Pmk1 in cell invasion by *M. oryzae*, we decided to suppress host immune reactions simultaneous with Pmk1 inhibition. We found that chemical suppression of plant ROS or disruption of salicylic acid regulation did not rescue the effects of Pmk1 inactivation (see fig S9 for details). To suppress host immunity completely, we therefore killed plant tissue by ethanol treatment, before rehydration and inoculation with the *pmk1*^{AS} mutant. In the presence of 1NA-PP1, the mutant still remained trapped in the first dead plant cell (Fig 4A). We therefore hypothesized that Pmk1-dependent hyphal constriction must be critical for cell wall crossing at pit fields. This would be consistent with the role of Pmk1 in septin-dependent appressorium repolarization (fig S5) (*3, 13*). Consistent with this idea, RNA-seq analysis revealed several morphogenetic regulators down-regulated during Pmk1 inhibition. Chm1, a homologue of Cla4 PAK kinase, which phosphorylates septins (*22*), and a putative F-actin crosslinking protein, alpha-actinin, for

example, are among genes positively regulated by Pmk1 during plant infection (Table S2). We therefore investigated septin organisation during Pmk1 inhibition. Sep5-GFP still accumulated at cell wall contact points, but as a disorganized mass, instead of the septin collars that normally form at cell wall crossing sites (Fig 4, fig S10 and S11, and movie S3 and S5). Finally, we investigated the ability of septin mutants to invade plant tissue. Septin mutants do not penetrate rice cuticle efficiently due to their role in appressorium re-polarization and penetration hypha development (*3*). However, a small proportion of penetration events are successful. In these rare instances, the Δ*sep6* mutant, in particular, showed a reduction in its ability to spread between rice cells, consistent with septins playing a role in cell invasion (fig.S12).

Taken together, our results demonstrate that the Pmk1 MAPK pathway controls plant tissue invasion by controlling the constriction of invasive hyphae to traverse pit fields in order to invade new rice cells, while maintaining cellular integrity of the host. To accomplish this feat, the MAPK also regulates expression of a battery of effectors to suppress plant immunity, thereby preventing plasmodesmatal closure until the fungus has invaded neighboring cells. Plant tissue invasion by the blast fungus is therefore orchestrated, rapid, and necessary for the devastating consequences of the disease.

References:

1. R. A. Wilson, N. J. Talbot, Under pressure: investigating the biology of plant infection by Magnaporthe oryzae. *Nature Reviews Microbiology* **7**, 185-195 (2009).
2. Y. Inoue *et al.*, Evolution of the wheat blast fungus through functional losses in a host specificity determinant. *Science* **357**, 80-83 (2017).
3. Y. F. Dagdas *et al.*, Septin-mediated plant cell invasion by the rice blast fungus, Magnaporthe oryzae. *Science* **336**, 1590-1595 (2012).
4. C. Veneault-Fourrey, M. Barooah, M. Egan, G. Wakley, N. J. Talbot, Autophagic fungal cell death is necessary for infection by the rice blast fungus. *Science* **312**, 580-583 (2006).
5. M. C. Giraldo *et al.*, Two distinct secretion systems facilitate tissue invasion by the rice blast fungus Magnaporthe oryzae. *Nat Commun* **4**, 1996 (2013).
6. C. H. Khang *et al.*, Translocation of Magnaporthe oryzae effectors into rice cells and their subsequent cell-to-cell movement. *Plant Cell* **22**, (2010).
7. S. Mochizuki, E. Minami, Y. Nishizawa, Live-cell imaging of rice cytological changes reveals the importance of host vacuole maintenance for biotrophic invasion by blast fungus, Magnaporthe oryzae. *MicrobiologyOpen* **4**, 952-966 (2015).
8. G. Mosquera, M. C. Giraldo, C. H. Khang, S. Coughlan, B. Valent, Interaction transcriptome analysis identifies Magnaporthe oryzae BAS1-4 as biotrophy-associated secreted proteins in rice blast disease. *The Plant Cell* **21**, 1273-1290 (2009).
9. P. Kankanala, K. Czymmek, B. Valent, Roles for rice membrane dynamics and plasmodesmata during biotrophic invasion by the blast fungus. *The Plant Cell* **19**, 706-724 (2007).
10. K. Jones, D. W. Kim, J. S. Park, C. H. Khang, Live-cell fluorescence imaging to investigate the dynamics of plant cell death during infection by the rice blast fungus Magnaporthe oryzae. *BMC Plant Biology* **16**, 1-8 (2016).
11. C. Cheval, C. Faulkner, Plasmodesmal regulation during plant–pathogen interactions. *New Phytologist* 217, 62-67 (2018)
12. C. Faulkner *et al.*, LYM2-dependent chitin perception limits molecular flux via plasmodesmata. *Proceedings of the National Academy of Sciences* **110**, 9166-9170 (2013).
13. L. S. Ryder *et al.*, NADPH oxidases regulate septin-mediated cytoskeletal remodeling during plant infection by the rice blast fungus. *Proceedings of the National Academy of Sciences* **110**, 3179-3184 (2013).
14. W. Cui, J. Y. Lee, Arabidopsis callose synthases CalS1/8 regulate plasmodesmal permeability during stress. *Nature plants* **2**, 16034 (2016).

15. J.-R. Xu, J. E. Hamer, MAP kinase and cAMP signaling regulate infection structure formation and pathogenic growth in the rice blast fungus Magnaporthe grisea. *Genes & development* **10**, 2696-2706 (1996).
16. A. C. Bishop *et al.*, A chemical switch for inhibitor-sensitive alleles of any protein kinase. *Nature* **407**, 395-401 (2000).
17. K. S. Bruno, F. Tenjo, L. Li, J. E. Hamer, J.-R. Xu, Cellular localization and role of kinase activity of PMK1 in Magnaporthe grisea. *Eukaryotic Cell* **3**, 1525-1532 (2004).
18. K. P. Dixon, J.-R. Xu, N. Smirnoff, N. J. Talbot, Independent signaling pathways regulate cellular turgor during hyperosmotic stress and appressorium-mediated plant infection by Magnaporthe grisea. *The Plant Cell* **11**, 2045-2058 (1999).
19. J.-R. Xu, C. J. Staiger, J. E. Hamer, Inactivation of the mitogen-activated protein kinase Mps1 from the rice blast fungus prevents penetration of host cells but allows activation of plant defense responses. *Proceedings of the National Academy of Sciences* **95**, 12713-12718 (1998).
20. X. Zhang, W. Liu, Y. Li, G. Li, J. R. Xu, Expression of HopAI interferes with MAP kinase signalling in Magnaporthe oryzae. *Environ Microbiol* **19**, 4190-4204 (2017).
21. T. A. Mentlak *et al.*, Effector-mediated suppression of chitin-triggered immunity by magnaporthe oryzae is necessary for rice blast disease. *Plant Cell* **24**, 322-335 (2012).
22. L. Li, C. Xue, K. Bruno, M. Nishimura, J.-R. Xu, Two PAK kinase genes, CHM1 and MST20, have distinct functions in Magnaporthe grisea. *Molecular plant-microbe interactions* **17**, 547-556 (2004).
23. H. Leung *et al.*, Transformation of the rice blast fungus Magnaporthe grisea to hygromycin B resistance. *Current genetics* **17**, 409-411 (1990).
24. N. J. Talbot, D. J. Ebbole, J. E. Hamer, Identification and characterization of MPG1, a gene involved in pathogenicity from the rice blast fungus Magnaporthe grisea. *The Plant Cell* **5**, 1575-1590 (1993).
25. J. Sambrook, E. F. Fritsch, T. Maniatis, *Molecular cloning: a laboratory manual*. (Cold spring harbor laboratory press, 1989).
26. T. J. Penn *et al.*, Protein kinase C is essential for viability of the rice blast fungus Magnaporthe oryzae. *Molecular microbiology* **98**, 403-419 (2015).
27. A. H. Christensen, P. H. Quail, Ubiquitin promoter-based vectors for high-level expression of selectable and/or screenable marker genes in monocotyledonous plants. *Transgenic research* **5**, 213-218 (1996).
28. G. Doehlemann *et al.*, Pep1, a secreted effector protein of Ustilago maydis, is required for successful invasion of plant cells. *PLoS Pathog* **5**, e1000290 (2009).
29. J. Schindelin *et al.*, Fiji: an open-source platform for biological-image analysis. *Nature methods* **9**, 676-682 (2012).
30. M.-H. Chi, S.-Y. Park, S. Kim, Y.-H. Lee, A novel pathogenicity gene is required in the rice blast fungus to suppress the basal defenses of the host. *PLoS Pathog* **5**, e1000401 (2009).
31. C. Hacker, M. Howell, D. Bhella, J. Lucocq, Strategies for maximizing ATP supply in the microsporidian Encephalitozoon cuniculi: direct binding of mitochondria to the parasitophorous vacuole and clustering of the mitochondrial porin VDAC. *Cellular microbiology* **16**, 565-579 (2014).
32. R. A. Dean *et al.*, The genome sequence of the rice blast fungus Magnaporthe grisea. *Nature* **434**, 980-986 (2005).
33. D. Kim *et al.*, TopHat2: accurate alignment of transcriptomes in the presence of insertions, deletions and gene fusions. *Genome biology* **14**, 1 (2013).
34. C. Trapnell *et al.*, Differential gene and transcript expression analysis of RNA-seq experiments with TopHat and Cufflinks. *Nature protocols* **7**, 562-578 (2012).
35. E. Alonso-Rodriguez, P. Fernandez-Pinar, A. Sacristan-Reviriego, M. Molina, H. Martin, An Analog-sensitive Version of the Protein Kinase Slt2 Allows Identification of Novel Targets of the Yeast Cell Wall Integrity Pathway. *The Journal of biological chemistry* **291**, 5461-5472 (2016).
36. C. W. Mims, E. A. Richardson, B. F. Holt Iii, J. L. Dangl, Ultrastructure of the host–pathogen interface in Arabidopsis thaliana leaves infected by the downy mildew Hyaloperonospora parasitica. *Canadian Journal of Botany* **82**, 1001-1008 (2004).
37. X. Wang *et al.*, Salicylic acid regulates plasmodesmata closure during innate immune responses in Arabidopsis. *The Plant Cell* **25**, 2315-2329 (2013).
38. Y. Yang, M. Qi, C. Mei, Endogenous salicylic acid protects rice plants from oxidative damage caused by aging as well as biotic and abiotic stress. *The Plant Journal* **40**, 909-919 (2004).
39. A. Conesa, S. Götz, Blast2GO: A Comprehensive Suite for Functional Analysis in Plant Genomics. *International Journal of Plant Genomics* **2008**, 619832 (2008).
40. R. D. Finn *et al.*, The Pfam protein families database: towards a more sustainable future. *Nucleic acids research* **44**, D279-285 (2016).

Acknowledgements:

We thank Satoko Yoshida (RIKEN, Japan) for providing Nipponbare and NahG rice lines. **Funding**. This work was funded by a Halpin Scholarship for rice blast research to WS, a European Research Council, Advanced Investigator Award to NJT under the

European Union's Seventh Framework Programme (*FP7/2007-2013)* / ERC grant agreement n° 294702 GENBLAST, and Agriculture and Food Research Initiative Competitive Grant no. 2012-67013-19291 to BV from the USDA National Institute of Food and Agriculture. Contribution number 18-174-J from the Kansas Agricultural Experiment Station. **Author Contributions:** The project was conceived by WS, BV and NJT. WS, MOR, and EOG performed experimental work. DMS provided bioinformatic data analysis, GRJ carried out laser confocal imaging, CH and AC performed ultrastructural analysis, WS, MOR, BV and NJT wrote the paper with assistance and input of all co-authors. Competing Interests. The authors declare no competing interests. **Data and Materials Availability:** All data are available in the manuscript or the supplementary material. Differential gene expression analysis can be accessed at Gene Expression Omnibus (GEO) (https://www.ncbi.nlm.nih.gov/geo/), accession number GSE106845.

List of Supplementary materials:

Material and Methods

Figures S1-S13

Table S1- S2

Movie S1 to S5

References (*22-40*)

Fig. 1. Cell-to-cell invasion and plasmodesmatal manipulation by *M. oryzae*. (A) Transmission electron micrograph of invasive hypha (IH) traversing a rice cell wall (RCW) at 42 hours post-inoculation (hpi). Bar = 0.5 µm. **(B)** High magnification view of the crossing site. The rice plasma membrane (RPM), fungal plasma membrane (FPM) and fungal cell wall (FCW) are indicated. Bar = 20 nm. **(C)** Callose deposition in an infected rice cell 34 hpi, shown by aniline blue staining. Arrowheads indicate plasmodesmatal callose deposition. Arrows indicate callose collars that form around hyphae after they enter adjacent cells (asterisks). Bar = 5 µm. **(D)** Hyphae traversing cell wall at a pit field (white arrow). Bar = 0.5 µm. **(E)** Difference in host cytoplasmic contents between first- and second-invaded cells (for larger image see fig S1G). VC, vacuole. Bar = 1 µm. **(F)** Localisation of a septin Sep5-GFP collar at rice cell crossing points (white arrows and high magnification inset) at 40 hpi. Bar = 10 µm. Inset bar = 5 µm. **(G)** Diffusion of single or double mCherry fluorescent proteins in non-infected leaf tissue (left and middle panels, respectively), and in leaves infected by *M. oryzae* at 24 h (right panel) (*9*). Asterisks indicate bombarded cells. Bar = 10 µm. **(H)** Percentage of bombarded cells showing diffusion of mCherry proteins in blast-infected and non-infected rice tissue (**P* = 0.05; *n* = 100 cells).

Fig. 2. Pmk1 MAPK-dependent regulation of cell-to-cell spread by *M. oryzae.* (A) and **(B)** Effect of Pmk1 inhibition on host colonization at 48 hpi. Infected rice tissues were treated with 5 µM 1NA-PP1 at 26 hpi. Asterisks indicate appressorial penetration sites. **(C)** Formation of swollen hyphae by *pmk1*^{AS} mutant contacting host cell wall in the presence of 1NA-PP1, imaged at 40 hpi. **(D)** and **(E)** Induction of ROS production, shown by 3,3'-diaminobenzidine (DAB) staining, after adding 1NA-PP1 at 26 hpi, imaged at 48 hpi. *n* = 300 infection sites; **P* < 0.05, ***P* < 0.01. ****P* < 0.001; unpaired Student's *t* test. Bar = 20 µm. **(F)** Transient accumulation of Pmk1-GFP in an appressorium during emergence of a penetration hypha. **(G)** Transient accumulation of Pmk1-GFP in hyphae at rice cell crossing points (asterisks).

Fig. 3. Pmk1-dependent regulation of effector gene expression during biotrophic growth. (A) Bar chart showing relative expression levels (fragments per kilobase of transcript per million mapped reads - FPKM) of known effector genes differentially regulated during Pmk1 inhibition by RNA-seq. **(B)** and **(C)** Localization of Bas2-GFP and Bas3-GFP effectors, respectively, in a *pmk1*^{AS} mutant ± 1NA-PP1. BICs are indicated by arrows. **(D)** to **(F)** Expression of cytosolic GFP driven by the *BAS3* promoter (Bas3p:GFP) in a *pmk1*^{AS} mutant. **(D)** At 24 hpi, appressoria undergoing infection showed strong GFP expression, while appressoria treated with 1NA-PP1 at 8 hpi did not. **(E)** GFP expression in *pmk1*^{AS} hyphae exposed to 1NA-PP1 at 26 hpi and imaged at 30 hpi. **(F)** Dot plot of Bas3p:GFP fluorescence in *pmk1*^{AS} mutant treated or untreated with 5 µM 1NA-PP1 at 26 hpi. Images were taken at 30 hpi, and background subtracted before measuring fluorescence levels. *****P* < 0.0001, unpaired Student's *t* test; three biological replicates. Bar = 20 µm.

Fig. 4 Pmk1 controls septin-dependent morphogenesis of narrow invasive hyphae traversing cell walls. (A) Micrographs to show *pmk1*^{AS} mutant, growing in ethanol-killed rice tissue treated with 1NA-PP1 at 14 hpi, remains trapped inside initially invaded rice cells in all 200 infection sites examined at 48 hpi. Asterisks indicate appressorium penetration sites. Bar = 20 μm **(B)** Confocal micrographs showing localization of Sep5-GFP in a *pmk1*^{AS} mutant at 42 hpi ±1NA-PP1 (5 μM) added at 26 hpi. Arrows indicate accumulation of Sep5-GFP at rice cell contact points. Bar = 10 μm. Red arrows in high magnification insets panels show linescans used to generated corresponding fluorescence intensity distribution graphs.

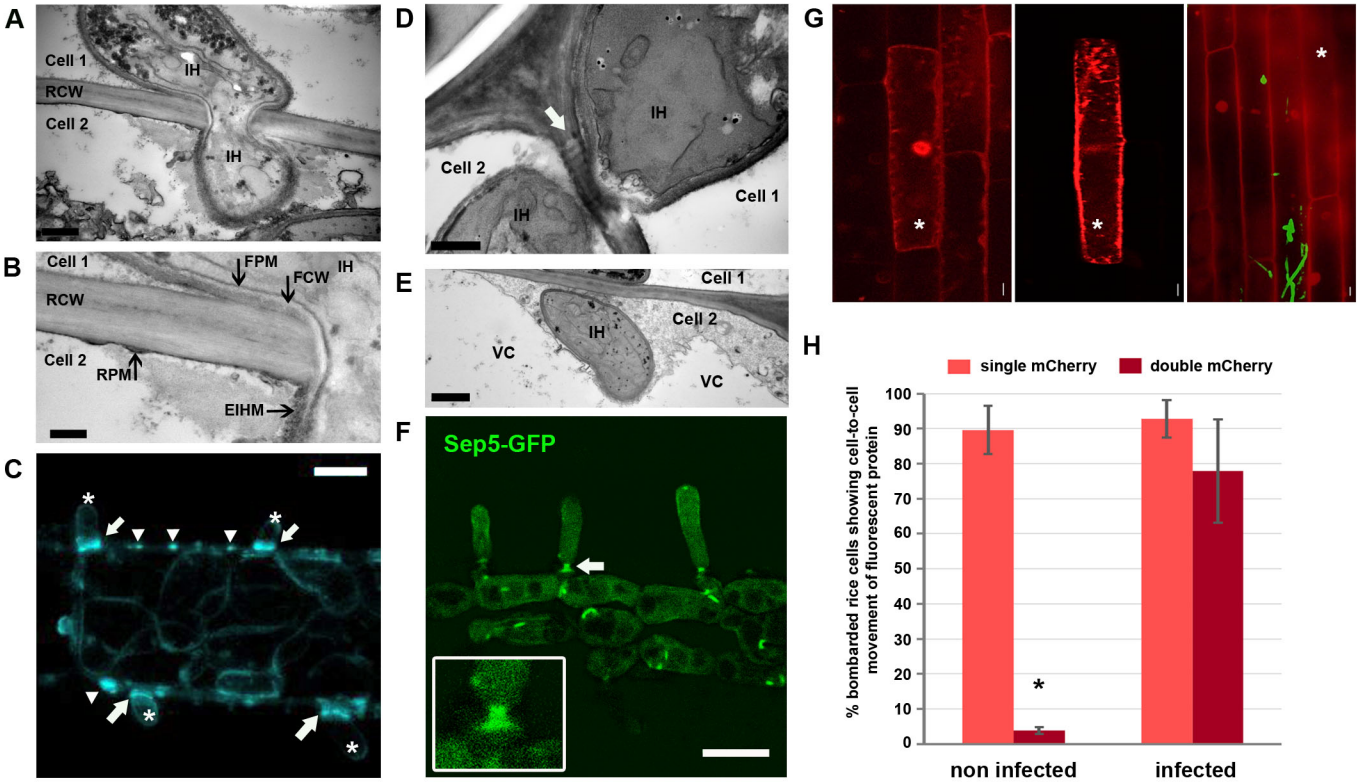

Fig. 1. Cell-to-cell invasion and plasmodesmatal manipulation by M. oryzae. (A) Transmission electron micrograph of invasive hypha (IH) traversing a rice cell wall (RCW) at 42 hours post-inoculation (hpi). Bar = 0.5 µm. (B) High magnification view of the crossing site. The rice plasma membrane (RPM), fungal plasma membrane (FPM) and fungal cell wall (FCW) are indicated. Bar = 20 nm. (C) Callose deposition in an infected rice cell 34 hpi, shown by aniline blue staining. Arrowheads indicate plasmodesmatal callose deposition. Arrows indicate callose collars that form around hyphae after they enter adjacent cells (asterisks). Bar = 5 µm. (D) Hyphae traversing cell wall at a pit field (white arrow). Bar = 0.5 µm. (E) Difference in host cytoplasmic contents between first- and second-invaded cells (for larger image see fig S1G). VC, vacuole. Bar = 1 µm. (F) Localisation of a septin Sep5-GFP collar at rice cell crossing points (white arrows and high magnification inset) at 40 hpi. Bar = 10 µm. Inset bar = 5 µm. (G) Diffusion of single or double mCherry fluorescent proteins in non-infected leaf tissue (left and middle panels, respectively), and in leaves infected by M. oryzae at 24 h (right panel) (9). Asterisks indicate bombarded cells. Bar = 10 µm. (H) Percentage of bombarded cells showing diffusion of mCherry proteins in blast-infected and non-infected rice tissue (*P = 0.05; n = 100 cells).

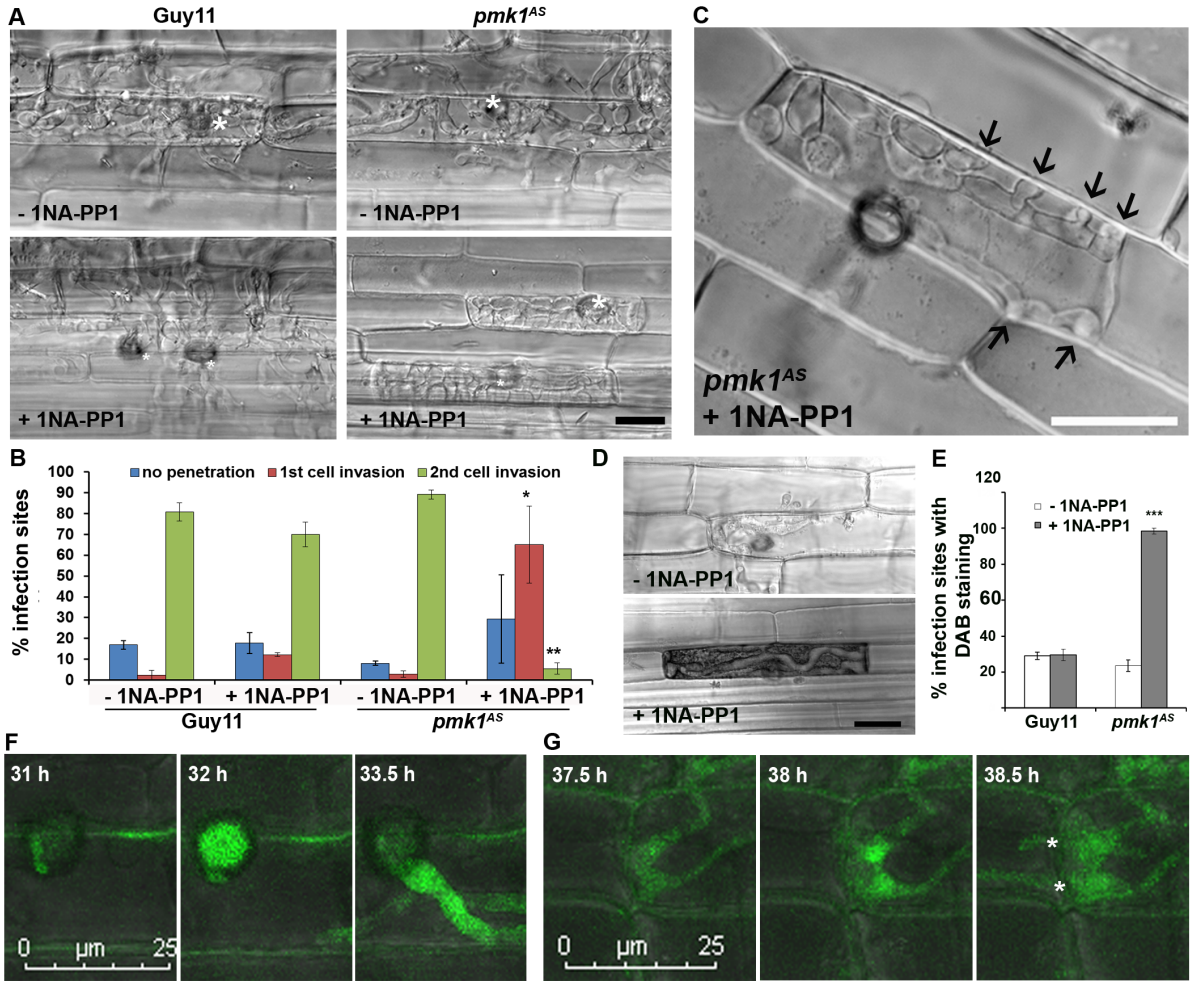

Fig. 2. Pmk1 MAPK-dependent regulation of cell-to-cell spread by *M. oryzae*. **(A)** and **(B)** Effect of Pmk1 inhibition on host colonization at 48 hpi. Infected rice tissues were treated with 5 µM 1NA-PP1 at 26 hpi. Asterisks indicate appressorial penetration sites. **(C)** Formation of swollen hyphae by *pmk1*^{AS} mutant contacting host cell wall in the presence of 1NA-PP1, imaged at 40 hpi. **(D)** and **(E)** Induction of ROS production, shown by 3,3'-diaminobenzidine (DAB) staining, after adding 1NA-PP1 at 26 hpi, imaged at 48 hpi. $n = 300$ infection sites; $^{*}P < 0.05$, $^{**}P < 0.01$. $^{***}P < 0.001$; unpaired Student's t test. Bar = 20 µm. **(F)** Transient accumulation of Pmk1-GFP in an appressorium during emergence of a penetration hypha. **(G)** Transient accumulation of Pmk1-GFP in hyphae at rice cell crossing points (asterisks).

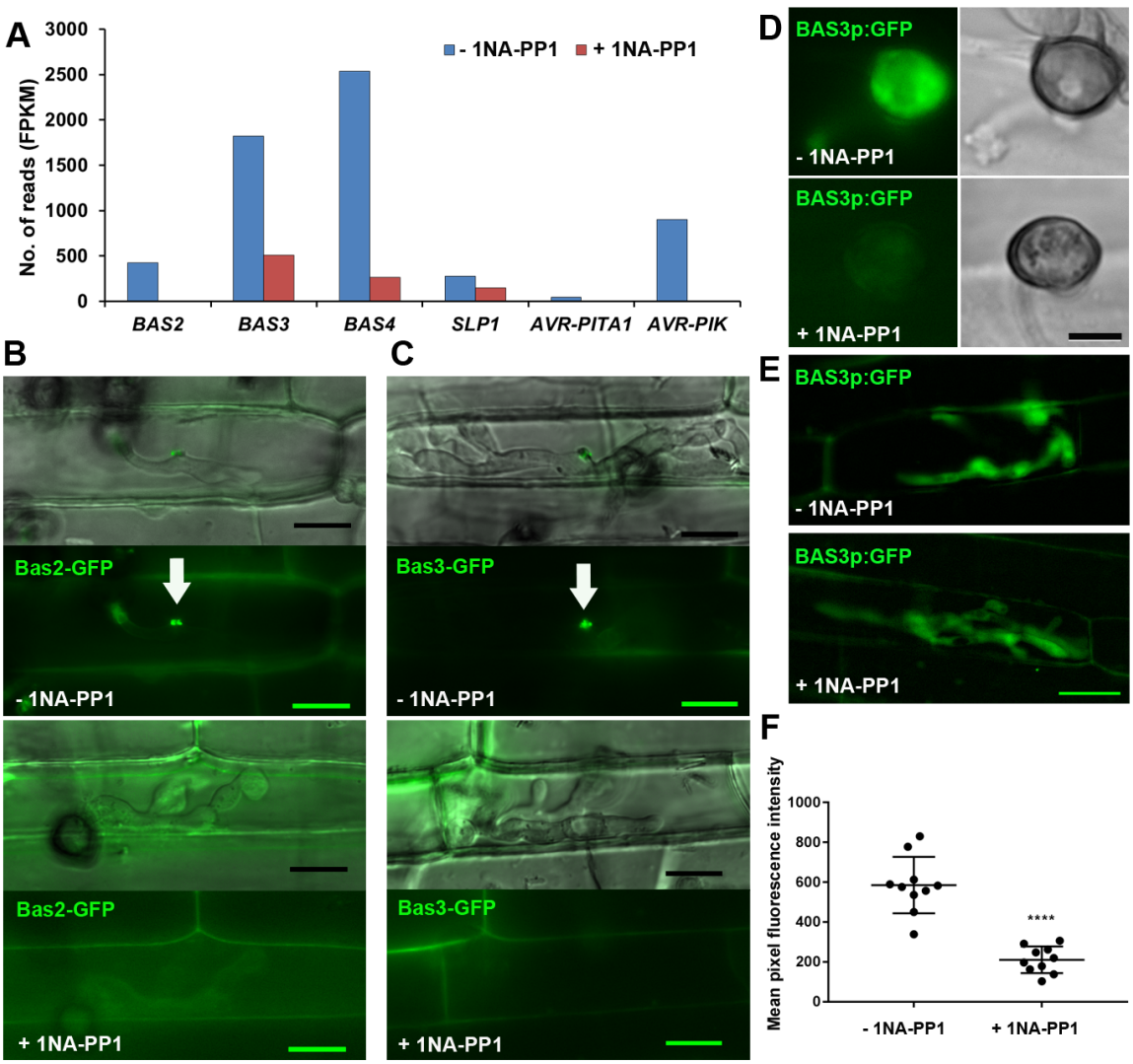

Fig. 3. Pmk1-dependent regulation of effector gene expression during biotrophic growth. (A) Bar chart showing relative expression levels (fragments per kilobase of transcript per million mapped reads - FPKM) of known effector genes differentially regulated during Pmk1 inhibition by RNA-seq. **(B)** and **(C)** Localization of Bas2-GFP and Bas3-GFP effectors, respectively, in a *pmk1*^{AS} mutant ± 1NA-PP1. BICs are indicated by arrows. **(D)** to **(F)** Expression of cytosolic GFP driven by the *BAS3* promoter (Bas3p:GFP) in a *pmk1*^{AS} mutant. **(D)** At 24 hpi, appressoria undergoing infection showed strong GFP expression, while appressoria treated with 1NA-PP1 at 8 hpi did not. **(E)** GFP expression in *pmk1*^{AS} hyphae exposed to 1NA-PP1 at 26 hpi and imaged at 30 hpi. **(F)** Dot plot of Bas3p:GFP fluorescence in *pmk1*^{AS} mutant treated or untreated with 5 µM 1NA-PP1 at 26 hpi. Images were taken at 30 hpi, and background subtracted before measuring fluorescence levels. ****$P <$ 0.0001, unpaired Student's *t* test; three biological replicates. Bar = 20 µm.

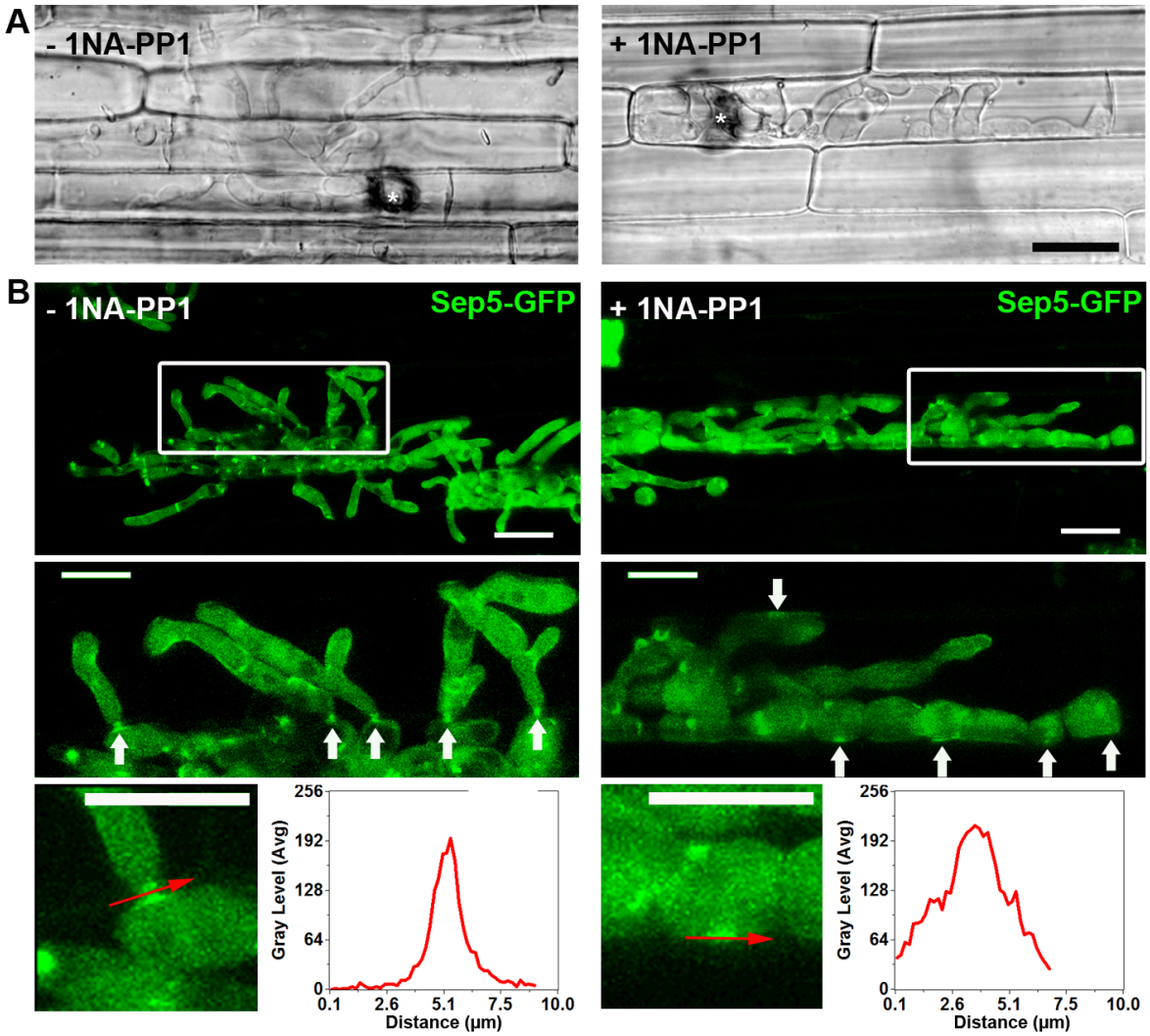

Fig. 4 Pmk1 controls septin-dependent morphogenesis of narrow invasive hyphae traversing cell walls. (A) Micrographs to show *pmk1*^{AS} mutant, growing in ethanol-killed rice tissue treated with 1NA-PP1 at 14 hpi, remains trapped inside initially invaded rice cells in all 200 infection sites examined at 48 hpi. Asterisks indicate appressorium penetration sites. Bar = 20 µm **(B)** Confocal micrographs showing localization of Sep5-GFP in a *pmk1*^{AS} mutant at 42 hpi ±1NA-PP1 (5 µM) added at 26 hpi. Arrows indicate accumulation of Sep5-GFP at rice cell contact points. Bar = 10 µm. Red arrows in high magnification insets panels show linescans used to generated corresponding fluorescence intensity distribution graphs.

Supplementary materials:

Materials and Methods:

Fungal strains, growth conditions, pathogenicity and infection-related development assays, inhibitor treatment and DNA analysis

All fungal strains used in this study are derived from the Guy11 wild type or Δ*pmk1* strains of *Magnaporthe oryzae* (*15, 23, 24*). Standard protocols for fungal growth, maintenance, transformation, appressorium development assay, pathogenicity assays and DNA extraction were performed, as described previously (*24*). Restriction digestion, Southern blot analysis, polymerase chain reaction (PCR) and DNA sequencing were carried out using standard procedures (*25*). Observations of plant penetration and *in planta* growth were performed using the rice blast susceptible CO-39 rice cultivar (*24*) using leaf sheath assays, as described previously (*9*). A suspension of 10^5 spores per mL was prepared in 0.2% gelatin and injected into the hollow space of the rolled-up leaf sheath tissue prepared from 3-4 week-old rice seedlings. The inner epidermis of the leaf sheath tissue, where the fungus grows, was trimmed, mounted and observed by light, epifluoresecence of laser confocal micoscopy. The ATP analogue 1NA-PP1 was chemically synthesized, as previously described (*26*). The 2,3-DMB-PP1 analogue was purchased from Santa Cruz Biotechnology. Stock solutions of 1NA-PP1 and 2,3-DMB-PP1 were prepared in 100% DMSO to a final concentration of 10 mM, and kept at -20 °C. Working solutions of the ATP analogues were diluted in distilled water to the required concentration, normally 5μM. Dead rice leaf tissue was prepared by immersing rice leaf sheath in 100% ethanol overnight, followed by rehydration in distilled water for 6 hours prior to inoculation with fungal conidia.

Tissue bombardment assay for transient expression of mCherry fluorescent protein in rice tissue

In order to generate the single mCherry bombardment vector, p123-potef-PUBI:mCherry, the 2017-bp maize Ubiquitin promoter was obtained from pAHC17 (*27*) by *Hin*dIII and *Bam*H1 digestion, gel purified and cloned into p123-potef-mCherry (*28*). The vector for expressing double-sized mCherry fusion protein was generated by amplification of the 708-bp mCherry fragment from p123-potef-mCherry using primers NcoI_mCherry-Fw and NcoI_mCherry-Rv, and cloning this fragment into the *Nco*I site of the Single mCherry bombardment vector, resulting in vector p123-potef-PUBI:2xmCherry. Leaf sheath tissue was prepared from three week old rice plants (cv.YT16) and bombarded individually with p123-potef-PUBI:mCherry and p123-potef-PUBI:2xmCherry plasmids using a particle inflow gun (Bio-Rad). Infected sheath tissues were bombarded at 24 hours post inoculation. After 24 hours, leaf sheaths were trimmed and diffusion of the fluorescent proteins evaluated by laser confocal microscopy. Confocal imaging was performed with a Zeiss LSM780 confocal microscope system using two water immersion

objectives, C-Apochromat 40x/1.2 W Corr and C-Apochromat 40x/1.2WCorr. Images were acquired and processed using ZEN 2010 software.

Generation of analogue-sensitive *pmk1*^{AS} and *mps1*^{AS} mutants and GFP fusion constructs

The analogue-sensitive allele of *PMK1*, harbouring a Q104G mutation, was generated using site-directed mutagenesis and sub-cloned into pCB1532 plasmid carrying sulfonylurea resistance gene *ILV1* (GenBank; AF013601) using conventional DNA cloning procedures (*25*). The resulting *pmk1*^{AS} plasmid was introduced into the Δ*pmk1* mutant (*15*), and fungal transformants containing a single copy insertion were identified by Southern blot analysis (*24*). The analogue-sensitive allele of *MPS1* (MGG_04943), harbouring a E186G mutation, was generated using site-directed mutagenesis and sub-cloned into pNEB1284 plasmid with a bialaphos resistance cassette using In-Fusion HD Cloning method (Takara). The *mps1*^{AS} plasmid was integrated into an Δ*mps1* mutant (*18*), and fungal transformants containing a single copy insertion were identified by Southern blot analysis. Generation of translational GFP fusions were carried out by the homologous recombination cloning method using the In-Fusion HD Cloning Kit (Clontech). Routinely, 2 kb native, endogenous promoter fragments were identified and amplified either with, or without, the corresponding gene coding sequence using primers designed to introduce 15 bp extensions which overlapped with adjacent fragments, allowing the ends to fuse during In-Fusion HD Cloning. All positive clones were identified by colony PCR and DNA sequencing. All constructs used in this study were verified by DNA sequencing and all fungal transformants verified by Southern blot analysis to ensure they were single copy insertions. Routinely, 3-4 transformants were observed for each construct used to ensure uniform representative results. All the primers used in this study are listed in Supplementary Table 1.

Light microscopy, tissue staining and electron microscopy

Conventional epifluorescence and differential interference contrast (DIC) microscopy was performed on an IX81 motorized inverted microscope (Olympus, Hamburg, Germany). A Photometrics CoolSNAP HQ2 camera system (Roper Scientific, Germany) under the control of MetaMorph software package (MDS Analytical Technologies, Winnersh, UK) was used to capture images from the microscope. Confocal laser scanning fluorescence microscopy was performed on a Leica TCS SP8 microscope using a 40x oil immersion objective lens. Image analysis was performed using the MetaMorph 7.5 Software (Molecular Devices, Dawnington, USA) and publically available Fiji software (*29*). *In situ* hydrogen peroxide detection was performed as described (*30*). An aqueous solution of 1 mg mL^{-1} of 3,3'-diaminobenzidine (DAB) in 10 mM Na_2HPO_4 was added from the edge of the cover glass to previously mounted leaf sheath tissue on the glass slide. Tissue was incubated for 4 h at room temperature to allow oxidization of DAB. Insoluble brown precipitate was observed under standard light microscopy. For visualization of callose deposition, aniline blue (0.1 mg mL^{-1}) solution was prepared in 150 mM KH_2PO_4 and added to pre-mounted rice tissue for up to 30 min before rinsing with water and imaging by laser confocal scanning microscopy. The aniline

blue fluorochrome was excited with a 405-nm laser and collected at 440–490-nm (*12*). For ultrastructural studies, a transmission electron microscopy procedure was modified from a previously described method (*31*). Briefly, small pieces of infected rice leaf sheaths were fixed in 5% glutaraldehyde and 4% formaldehyde in 0.05M sodium cacodylate buffer (pH 7.2). The first 5 min of fixation was performed under a mild vacuum, followed by 2 h incubation at room temperature. After 3 x 5 min washes in buffer the samples were post-fixed for 90 min in 1% osmium tetroxide reduced with 1.5% potassium hexacyanoferrate in deionized water. Samples were then washed 3 x 5 min with deionized water before dehydrating the tissue through a graded ethanol series (from 30% to 100% ethanol, 10 min per step). Over the next 24 h the dehydrated samples were then embedded gradually in Spurr resin (TAAB, Aldermaston, UK) and allowed to polymerize at 65°C for 24 h. Then, 80 nm ultrathin sections were collected on pioloform-coated copper 100 mesh grids (Agar Scientific, Standsted, Essex, UK) and contrasted with Reynold's lead citrate for 10 min. Sections were analysed using a JEOL JEM 1400 transmission electron microscope operated at 120KV and images taken using an ES 100W CCD digital camera (Gatan, Abingdon, Oxon, UK). Consecutive 70 nm serial sections including complete cell-to-cell crossing sites were collected on copper slot grids and used to determine the maximum hyphal diameter passing through pit fields.

Transcriptional profile analysis of *M. oryzae* infected rice tissue

Rice leaf sheaths were inoculated with the *pmk1*^{AS} mutant. At 26 hpi, the infected rice sheaths were treated with 5 µM 1NA-PP1. A control set were inoculated with DMSO control solution. Three independent-biological replicates were performed for both treated and control sets of samples. At 32 hpi, infected rice sheath tissue was trimmed manually and total RNA extracted using the RNeasy Plant Mini Kit (QIAGEN). RNA-seq libraries were prepared using 5 µg of total RNA with TruSeq SBS Kit v3 from Illumina (Agilent) according to the manufacturer's instructions and 125 base paired-end reads generated using an Illumina HiSeq 2500 platform (Illumina, Inc.). Reads were filtered using the fastq-mcf program from the eautils package (http://code.google.com/p/ea-utils/) applying –x 0.01, –q 20, –p 10, and –u. Filtered reads were mapped to the *M. oryzae* 70-15 reference genome version 8 (*32*) using the TopHat2 splice site-aware aligner (*34*). The Cufflinks suite of programs was used to estimate relative transcript abundance, expressed as FPKM (Fragments per kilobase of transcript per million mapped reads) and to test for differential gene expression (*34*). Differential gene expression is tested using the q-value, which is the p-value adjusted for false discovery rate (FDR) due to multiple testing. A q-value of 0.05 suggests that 5% of significant tests will result in false positives. Raw reads and differential gene expression analysis can be accessed at Gene Expression Omnibus (GEO) (https://www.ncbi.nlm.nih.gov/geo/), accession number GSE106845.

Fig. S1. Cell wall crossing sites and interaction of *M. oryzae* with plasmodesmata. (A) to **(F)** Transmission Electron Micrographs to show invasive hyphae (IH) traversing rice cell walls (RCW) during tissue invasion by *M. oryzae*. Infected tissue samples were harvested at 42 hours post inoculation. **(A)** and **(B)** show a pit field crossing site with a visible plasmodesma (arrowed). **(C)** and **(D)** show the movement of IH from a thin-walled epidermal cell to a thick-walled sclerenchyma cell (left) without a pit field spotted in any serial sections at this crossing site. An angled arrow indicates accumulation of fungal secretory vesicles near the host wall contact site. **(E)** A hypha entering a new rice cell showing extra-invasive hyphal membrane and invaginated host tonoplast (TP) in the second invaded cell. Cytoplasmic contents of the second rice cell are more apparent than those in the first invaded cell. **(F)** A pit field site (arrowed) of a *M. oryzae*-infected rice cell. **(G)** A larger image from Figure 1E to highlight difference in cytoplasmic contents of first and second invaded rice cells. Tonoplast, TP, Vacuole, VC. Bars in **(A), (C)** and **(G)** = 1 µm. Bar in **(B)** = 0.2 µm. Bars in **(D)** to **(F)** = 0.5 µm.

Fig. S2. Time series images to show cell biology of rice tissue invasion by *M. oryzae*. (A) Time-series images to show localization of Pwl2-mCherry-NLS and Bas4-GFP. The apoplastic effector gene fusion Bas4-GFP was expressed under its native promoter in *M. oryzae* and initially outlines invasive hyphae during invasion of the initial epidermal cell. After 32h, when the fungus has entered the next cell, Bas4-GFP fluorescence is observed in the plant cytoplasm but did not diffuse into adjacent rice cells after the EIHM had collapsed (33h onwards), suggesting that by this time plasmodesmata in the initial infected rice cells are closed. **(B)** Time-series images to show morphological transition of fungal hyphae upon touching the host cell wall. A fungal actin-binding protein Gelsolin-GFP accumulated at hyphal constriction sites during cell-to-cell traversal (white arrows), consistent with the presence of acto-myosin contractile ring structures that preceded formation of fungal septa. Acto-myosin contractile ring structures are observed at each cell crossing point as the fungus invades rice tissue Bar = 10 µm. **(C)** The polarisome marker Spa2-GFP initially localizes to growing hyphal tips in invasive hyphae (black arrows pointing to the right), but disappear when hyphal tips make contact with host cell wall (white arrows). Spa2-GFP then re-appears at hyphal tips in the adjacent rice cell as it is invaded (black arrows pointing to the left). Bar = 25 µm.

Fig. S3. Dynamics of callose deposits and plasmodesmatal permeability during *M. oryzae* infection. Time course images showing an increase in plasmodesmatal callose deposition in a compatible interaction between *M. oryzae* and rice, over time. Leaf sheaths of CO-39 susceptible rice cultivar were inoculated with the Guy11 wild type strain. Aniline blue staining and laser confocal microscopy were then carried out at 27, 30 and 34 hpi. Three different forms of callose deposition are visible. First, a callose-rich papilla (P) is often visible underneath appressorium penetration sites. Secondly, callose collars form at cell wall crossing sites around invasive hyphae (arrowed). These collars form *after* traversal of the cell wall by *M. oryzae* hyphae in compatible interactions. Finally, callose deposition is observed at plasmodesmata in pit fields (marked by arrow heads). These

only become visible once *M. oryzae* has moved beyond the first epidermal cell, consistent with plasmodesmatal closure occurring only after this time, and the loss of viability of initially invaded cells. Bar = 20 µm.

Fig. S4. Introduction the *pmk1*^{AS} allele and selective disruption of *pmk1*^{AS} activity by an ATP analogue. (A) Expression of the *pmk1*^{AS} allele complemented the pathogenicity defects of the Δ*pmk1* mutant (*15*). A suspension of 1 x 10^5 conidia ml^{-1} was sprayed to whole rice plants of cultivar CO-39 (*24*). Lesion density was recorded after 5 days (n = 30 plants). **(B)** Addition of 1NA-PP1 to germinating conidia reduced appressorium formation by the *pmk1*^{AS} strain in a dose-dependent manner, while the Guy11 wild type was not affected. Bar = 20 µm. **(C)** Addition of 5 µM 1NA-PP1 at 4 hours or later did not affect appressorium development. *$P < 0.05$; ***$P < 0.001$ (unpaired Student's t test; three biological replicates; 300 spores observed), demonstrating the window of Pmk1 activity necessary for appressorium morphogenesis. **(D)** Leaf drop inoculation assay to show the effect of 1NA-PP1 addition on lesion formation by the *pmk1*^{AS} mutant.

Fig. S5. Pmk1 activity is required for septin-dependent appressorium-mediated cuticle penetration. (A) Micrographs to show the effect of Pmk1 inhibition on appressorium-mediated rice leaf penetration. Appressoria were treated with 5 µM 1NA-PP1 at 15 hpi and infections allowed to proceed until 30 hpi. Bar = 20 µm. **(B)** Bar chart to show the frequency of plant penetration after treatment with 5 µM 1NA-PP1 at different time points. **(C)** Septin ring assembly at the appressorium pore visualised by expression of Sep5-GFP under its native promoter (*3*). **(D)** Inhibition of Pmk1 resulted in mislocalisation of the septin ring in the appressorium pore of *pmk1*^{AS} mutants, resulting in diffused Sep5-GFP accumulation rather than a clear ring-shaped structure. Guy11 or *pmk1*^{AS} appressoria expressing Sep5-GFP developed on cover slips were treated with 5 µM 1NA-PP1 at 6 hours. Bar = 10 µm. **(E)** Bar chart to show the frequency of appressorium showing intact septin rings after appressoria were treated with 1NA-PP1 at 6 hours. *$P < 0.05$; **$P < 0.01$; ***$P < 0.001$; unpaired Student's t test; three biological replicates; 300 spores observed).

Fig. S6. Chemical genetic inactivation of Pmk1 prevents cell-to-cell invasion of different hosts by *M. oryzae*, and rapidly elicits ROS generation and ROS-dependent callose deposition. (A) Invasive hyphae of the *pmk1*^{AS} mutant at 30 hpi treated with 1NA-PP1 (a 5 µM concentration was added at 26 hpi for all experiments). Arrow indicates a BIC. **(B)** to **(C)** Pmk1 inhibition blocked second cell invasion in the blast-susceptible rice cultivar, Mokoto **(B)** and Golden Promise barley leaf sheaths **(C)**. **(D)** Detection of hydrogen peroxide in infected rice tissue at 30 hpi by DAB staining after addition of 1NA-PP1. **(E)** Representative laser confocal micrographs and quantification of plasmodesmatal callose deposition in rice cells infected with Guy11 or *pmk1*^{AS} strains treated with 1NA-PP1 at 26 hpi in the presence or absence of 0.4 µM DPI, an inhibitor of plant NADPH oxidases, added at 16 hpi, and recorded at 44 hpi. Callose deposition at plasmodesmata is a ROS-dependent process that can be inhibited by DPI. The presence of 1NA-PP1 has no significant effect on Guy11. Addition of 1NA-PP1 to the *pmk1*^{AS} mutant results in a significant increase in ROS-dependent callose deposition at plasmodesmata. This can be prevented by addition of

DPI. Callose collars at cell wall crossing points are not ROS-dependent and were visible in Guy11 and untreated samples. They were not counted. *$P < 0.05$; **$P < 0.01$; ****$P < 0.0001$; two-way ANOVA; three biological replicates; $n = 30$ infected cells. NS, no significant difference. All bars = 20 μm.

Fig. S7. Inactivation of the cell integrity MAPK Mps1 disrupted appressorium function but did not prevent cell-to-cell invasion in host tissue. The Mps1 MAPK is a functional homologue of yeast Slt2 that is essential for rice blast disease (*18*). We generated a *mps1*^{AS} mutant harbouring a E186G mutation based on the previously reported yeast Slt2-as allele (*35*). The *mps1*^{AS} mutant was inoculated on rice leaf sheaths, in the presence or absence of the ATP analogue 4-Amino-1-tert-butyl-3-(2,3-dimethylbenzyl)pyrazolo[3,4-d]pyrimidine (2,3-DMB-PP1) (20 μM) at 0 or 26 hpi, and observed at 48 hpi. Addition of 2,3-DMB-PP1 at 0 h disrupted appressorium morphogenesis and plant penetration by the *mps1*^{AS} mutant, but when the inhibitor was added at 26 hpi the mutant was able to invade neighboring rice cells. Infected rice cells containing *mps1*^{AS} hyphae showed granulation, indicating that the absence of Mps1 activity may elicit, or de-repress, host defense responses (*20*). Bar chart to show frequency of fungal developmental stage. $n = 300$ infection sites; ***$P < 0.001$; unpaired Student's t test; 300 infection sites observed. Bar = 20 μm.

Fig. S8. A sub-set of *M. oryzae* effectors are regulated in a Pmk1-dependent manner during plant infection. (A) Micrographs to show that the *pmk1*^{AS} strain expressing *BAS3p:GFP* did not show GFP fluorescence in appressoria formed on an unyielding artificial surface (left panel), or in an appressorium on a rice leaf surface prior to penetration (right panel), in the absence of 1NA-PP1. Expression was only observed after successful penetration, as shown in Fig. 3D **(B)** Representative epifluorescence micrographs to show localization of Bas1-GFP, Bas4-GFP, Slp1-GFP and PWL2-GFP effector gene fusions in a *pmk1*^{AS} mutant after addition of 1NA-PP1 at 26 hpi. Images were recorded at 32 hours, and selected from of at least 50 infection sites for each experiment. Merged DIC and GFP images are shown in top panels, and GFP signal alone is shown in lower panels. These data demonstrate that not all *M. oryzae* effectors are regulated by Pmk1, but rather that a sub-set of effectors depend on Pmk1 activity for expression during invasive growth. Bar = 20 μm.

Fig. S9. Inactivation of host defense responses does not rescue the defect in cell-to-cell invasive growth caused by selective inhibition of Pmk1. (A) Representative micrographs showing the effect of ROS inhibition in cell-to-cell movement of the *pmk1*^{AS} mutant. Infected rice sheaths were treated with 10 μM DPI, 100 μM manganese(*35*) tetrakis (1-methyl-4-pyridyl) porphyrin (MnTMPyP), a cell permeable superoxide dismutase mimetic, and the anti-oxidant 10 mM ascorbic acid, in the presence or absence of 5 μM 1NA-PP1 at 26 hpi, and observed at 48 hours. **(B)** Depletion of salicylic acid (SA) did not restore the ability of the *pmk1*^{AS} mutant to cross rice cell walls. Salicylic acid (SA) signaling has been shown to induce plasmodesmatal closure in *Arabidopsis thaliana* (*37*) and depletion of SA levels in rice enhances susceptibility to blast infection (*37*). The SA-deficient NahG transgenic rice line (*37*) and an untransformed wild type (WT) Nipponbare were therefore inoculated with the

pmk1^{AS} mutant. The ATP analogue 1NA-PP1 (5 μM) was then added to infected rice leaf sheaths at 26 hpi and infection progress assessed at 48 hpi. No second cell invasion was found in 1NA-PP1-treated *pmk1*^{AS} infections of the NahG rice line (n = 100 infection sites for each experiment). Bar = 20 μm .

Fig. S10. Time series images extracted from Movie S3 to show invasion of rice tissue and fungal septin dynamics in a *pmk1*^{AS} mutant in the absence of 1NA-PP1. Septin dynamics during rice infection by *M. oryzae* were visualized by laser scanning confocal microscopy of rice leaves infected with a *pmk1*^{AS} mutant expressing Sep5-GFP in the absence of 1NA-PP1 between 3-41 hpi**.** Invasion of adjacent cells can be clearly seen after 38hpi, rapidly moving to colonize rice tissue.

Fig. S11. Time series images extracted from Movie S5 to show entrapment of the *pmk1*^{AS} mutant treated with 1NA-PP1. Rice tissue was inoculated with a *pmk1*^{AS} mutant expressing Sep5-GFP under its native promoter and treated with 1NA-PP1. The mutant was unable to invade beyond the initially invaded rice cell and to send narrow hyphae into adjacent rice cells. The movie was made by visualizing Sep5-GFP localization between 31-37 hpi by laser confocal imaging.

Fig. S12. Fungal septins are involved in cell-to-cell invasion by invasive hyphae of *M. oryzae*. (A) Secondary cell invasion by the wild type strain Guy11 and the isogenic septin mutants, Δ*sep3-6* at 48 hpi (*3*). Asterisks indicate appressorium penetration sites. Bar = 20 μm. **(B)** Bar chart to show frequency of different stages of infection-related development at 48 hours (appressorium without penetration hyphae, first cell invasion and second cell invasion). n = 100 infection sites each experiment; $^{**}P < 0.01$; $^{***}P < 0.001$; unpaired Student's t test, comparing each development stage of each mutant strains with Guy11 wild type. The septin mutants are all impaired in virulence (*3*) and *Δsep3, Δsep5* and *Δsep6* mutants all show severe impairment in appressorium-mediated penetration. Following rare instances of successful appressorium-mediated infection, the *Δsep6* mutant, in particular, shows impairment in cell-to-cell invasion.

Fig. S13. Model for Pmk1 MAPK-mediated plant cell invasion. The Pmk1 MAPK is a central regulatory of invasive growth by the rice blast fungus *M. oryzae*. The signaling pathway controls the regulation of a sub-set of genes encoding secreted effectors that are involved in host immune suppression, particularly those that act at plasmodesmata. The MAPK pathway also regulates cellular morphogenesis of fungal invasive hyphae which undergo severe constriction as they cross plant cell walls during invasive growth, in order to cause rice blast disease.

Table S1 List of oligonucleotide primers used in this study

Primer	Oligonucleotide (5' to 3')
Pmk1AS-1	AGAATTCCAAGACCAACAAACAAAAAGAGTAGAAAA
Pmk1AS-2	CGGACTCCGATCAGGTACACCTCGTTGAA
Pmk1AS-3	CTACGAGACCTTCAACGAGGTGTACCTGATCGGAGTCCGTTGCTG CTGAACACTCCT
Pmk1AS-4	TGTGTGTTGGTTGTCGTTTAATTTATTTGAATTCA
Pmk1-ORF1	AAGCTGCTCCGGTACTTCAA
Pmk1-ORF2	GCTCCTATACGGTGGTCGAA
PMK1-GFP-P1	gagatttaggtcgacCAAGACCAACAAACAAAAAGAGTAGAAAA
Pmk1-GFP-P2	gcccttgctcaccatCCGCATAATTTCCTGGTAGATGAAC
V_Bar_F	CCGGGGGCGCGCCGCGTCGACAGAAGATGATATTGAAGG
Bar_Mps1_F	GAGATTTAGGTCGACTACCAAGACAAAAGAAAAAT
Mps1_mut2_F	CTATGGAGGTATGCACCCGCATTACATCAAGGATA
Mps1_mutR	GCGGGTGCATACCTCCATAGAGATAGGTCTCGTTG
V_MPS1utr_R	CGGCGCGCCGCGGCCATAAAGCAACGCATTTGTTTCCAG
Bas1-BARlink-P1	cgagatttaggtcgaCGTGAGGTCACGTGAGATC
Bas1-GFPlink-P2	gcccttgctcaccatCGGGTAATAATTCTCCACC
Bas2-Barlink-P1	gagatttaggtcgacCTTCGGCGACTTTGTCTTCCTC
Bas2-GFPlink-P2	gcccttgctcaccatGAAACCCTGCTTCTTGACCTGCTC
Bas3-Barlink P1	gagatttaggtcgacTTGAAAAAAGCCCCGTGG
Bas3-GFPlink P2	gcccttgctcaccatGTGGGCACTGTTGGCAGC
Bas3prom-GFP-P2	gcccttgctcaccatCTTGATGGTTGGGTTTTG
Bas4-Barlink P1	cgagatttaggtcgaGCTCCAAACTGCAATACTCGCT
Bas4-GFPlink P2	gcccttgctcaccatAGCAGGGGGGATAGACGAGCCA
Slp1-Barlink-P1	gagatttaggtcgacAGGAGGAAGATAGCCCAGC
Slp1-GFPlink-P2	gcccttgctcaccatGTTCTTGCAGATGGGGATG
Pwl2-BARlink-P1	cgagatttaggtcgaCGTCAGTGAACAAACCTGT
Pwl2-GFPlink-P2	gcccttgctcaccatCATAATATTGCAGCCCTCT
BASTA-P1	GCAGGCATGCAAGCTGTCGACAGAAGATGATATTGAAG

BASTA-P2	GTCGACCTAAATCTCGGTGAC
GFP-P1	ATGGTGAGCAAGGGCGAGGAGCTG
GFP-P2	CTTGTACAGCTCGTCCATGCCGTG
NcoI_mCherry-Fw	AACCATGGTGAGCAAGGGCGAGGAG
NcoI_mCherry-Rv	TTCCATGGTCTTGTACAGCTCGTCCATGC

Table S2 Expression level of fungal genes obtained from infected plant tissues in the presence or absence of 1NA-PP1, harvested at 32 hours post infection and analyzed by RNA-seq. The relative levels of transcript abundance are expressed as FPKM (Fragments Per Kilobase of transcript per Million mapped reads). Differential gene expression is tested using the q-value, which is the p-value adjusted for false discovery rate (FDR) due to multiple testing. A q-value of 0.05 suggests that 5% of significant tests will result in false positives. Annotation of *M. oryzae* genes was originally carried out at the Broad Institute (https://www.broadinstitute.org/scientific-community/science/projects/fungal-genome-initiative/magnaporthe-comparative-genomics-proj) but the data is now hosted at the Ensembl database (http://fungi.ensembl.org/Magnaporthe_oryzae/Info/Index). Genes were also functionally annotated using BLAST2GO (*39*) and Pfam (*40*). Genes with expression levels plotted in Figure S7 are highlighted in yellow. Raw reads and differential gene expression analysis can be accessed at the Gene Expression Omnibus (GEO) (https://www.ncbi.nlm.nih.gov/geo/) under accession number GSE106845.

Movie S1 Fungal actin dynamics during rice infection and cell wall crossing by *M. oryzae*, visualized by expression of Gelsolin-GFP in wild type strain Guy11. Rice leaves were infected and visualized by laser confocal microscopy between 30 and 47 hpi.

Movie S2 Dynamics of the sub-cellular localization patterns of fungal effectors during invasive growth in rice tissue, visualized by laser scanning confocal microscopy of Pwl2-mCherry and Bas4-GFP expressed in *M. oryzae* Guy11, between 28-36 hpi.

Movie S3 Septin dynamics during rice infection by *M. oryzae* visualized by laser scanning confocal microscopy of rice leaves infected with a *pmk1*^{AS} mutant expressing Sep5-GFP in the absence of 1NA-PP1 between 30-41 hpi**.** Invasion of adjacent cells can be clearly seen after 38 hpi, rapidly moving to colonize rice tissue.

Movie S4 Dynamics of Pmk1-GFP localization during appressorium penetration, fungal invasive growth and rice cell-to-cell movement by *M. oryzae*, visualized by laser scanning confocal microscopy of functional Pmk1-GFP expressed in a *Δpmk1* mutant between 30-44 hpi.

Movie S5 Movie to show fungal septin dynamics following selective inhibition of Pmk1. Rice tissue was inoculated with a *pmk1*^{AS} mutant expressing Sep5-GFP and treated with 1NA-PP1. The mutant was unable to invade beyond the initially invaded rice cell and to send narrow hyphae into adjacent rice cells. The movie was made by visualizing Sep5-GFP localization between 31-37 hpi by laser confocal imaging.

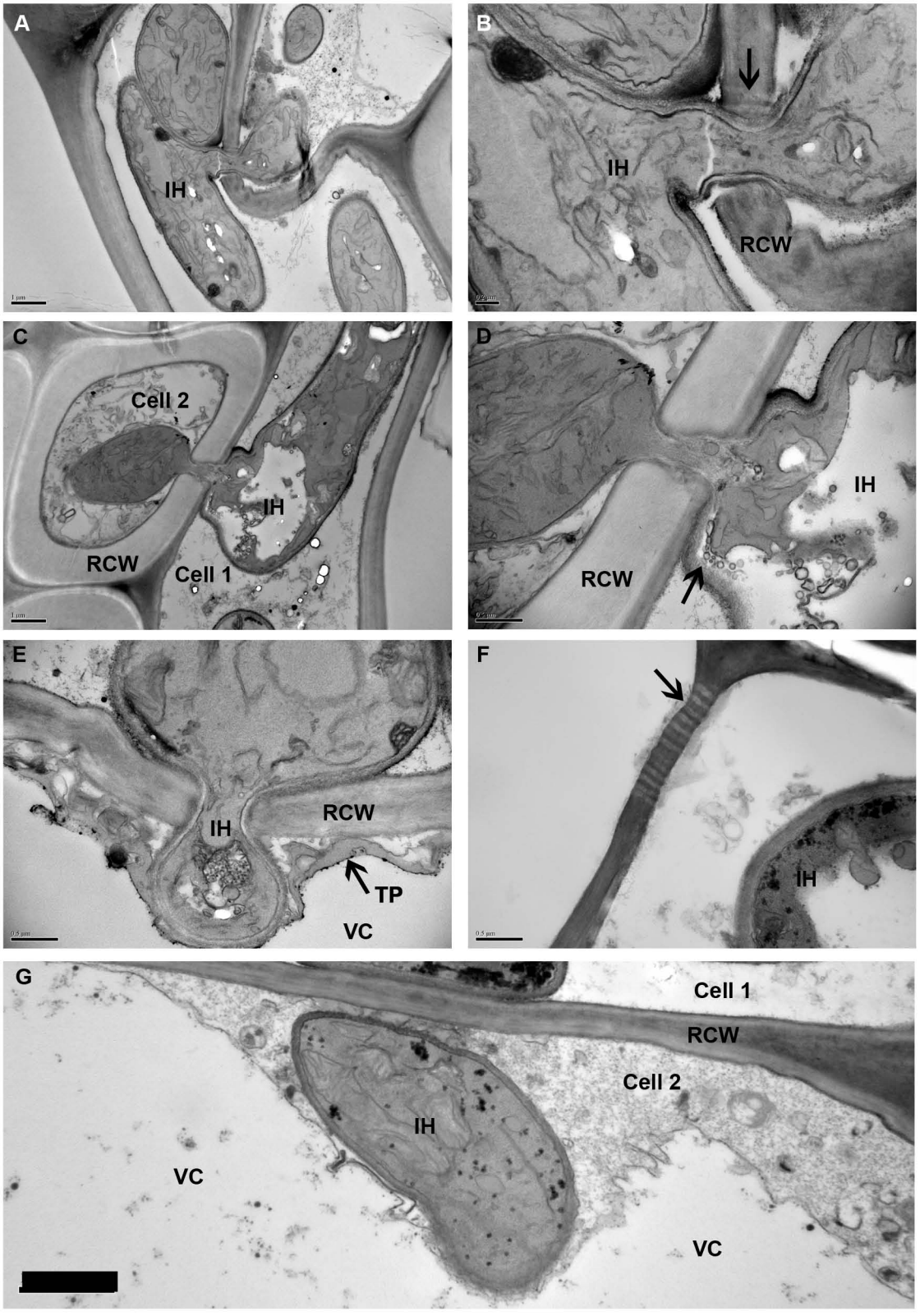
A
IH
B
IH
RCW
C
Cell 2
IH
RCW
Cell 1
D
IH
RCW
E
IH
RCW
TP
VC
F
IH
G
Cell 1
RCW
Cell 2
IH
VC
VC

Fig. S1. Cell wall crossing sites and interaction of *M. oryzae* with plasmodesmata. (A) to **(F)** Transmission Electron Micrographs to show invasive hyphae (IH) traversing rice cell walls (RCW) during tissue invasion by *M. oryzae*. Infected tissue samples were harvested at 42 hours post inoculation. **(A)** and **(B)** show a pit field crossing site with a visible plasmodesma (arrowed). **(C)** and **(D)** show the movement of IH from a thin-walled epidermal cell to a thick-walled sclerenchyma cell (left) without a pit field spotted in any serial sections at this crossing site. An angled arrow indicates accumulation of fungal secretory vesicles near the host wall contact site. **(E)** A hypha entering a new rice cell showing extra-invasive hyphal membrane and invaginated host tonoplast (TP) in the second invaded cell. Cytoplasmic contents of the second rice cell are more apparent than those in the first invaded cell. **(F)** A pit field site (arrowed) of a *M. oryzae*-infected rice cell. **(G)** A larger image from Figure 1E to highlight difference in cytoplasmic contents of first and second invaded rice cells. Tonoplast, TP, Vacuole, VC. Bars in **(A), (C)** and **(G)** = 1 µm. Bar in **(B)** = 0.2 µm. Bars in **(D)** to **(F)** = 0.5 µm.

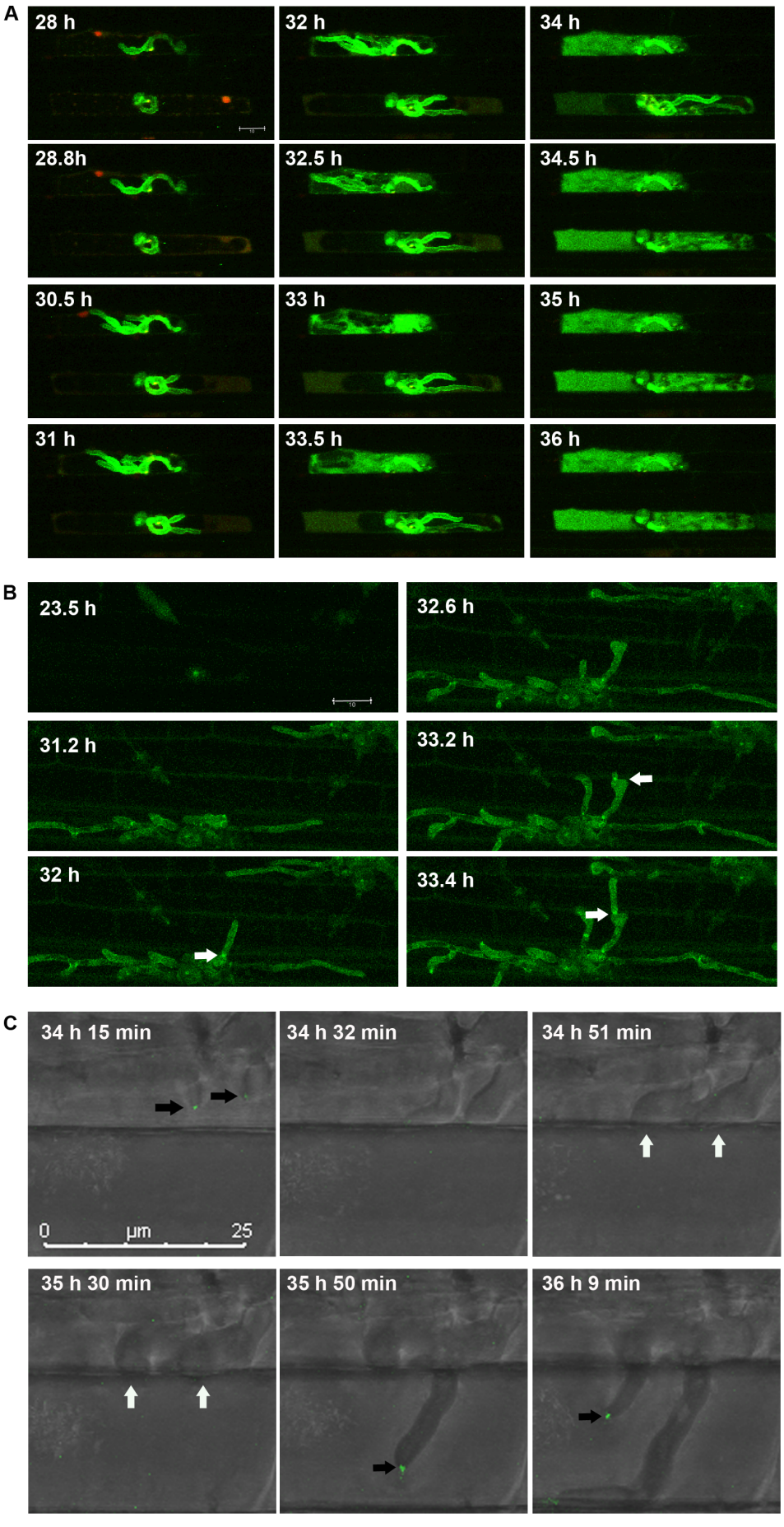
A
28 h
32 h
34 h
28.8h
32.5 h
34.5 h
30.5 h
33 h
35 h
31 h
33.5 h
36 h
B
23.5 h
32.6 h
31.2 h
33.2 h
32 h
33.4 h
C
34 h 15 min
34 h 32 min
34 h 51 min
0
µm
25
35 h 30 min
35 h 50 min
36 h 9 min

Fig. S2. Time series images to show cell biology of rice tissue invasion by *M. oryzae*. (A) Time-series images to show localization of Pwl2-mCherry-NLS and Bas4-GFP. The apoplastic effector gene fusion Bas4-GFP was expressed under its native promoter in *M. oryzae* and initially outlines invasive hyphae during invasion of the initial epidermal cell. After 32h, when the fungus has entered the next cell, Bas4-GFP fluorescence is observed in the plant cytoplasm but did not diffuse into adjacent rice cells after the EIHM had collapsed (33h onwards), suggesting that by this time plasmodesmata in the initial infected rice cells are closed. **(B)** Time-series images to show morphological transition of fungal hyphae upon touching the host cell wall. A fungal actin-binding protein Gelsolin-GFP accumulated at hyphal constriction sites during cell-to-cell traversal (white arrows), consistent with the presence of acto-myosin contractile ring structures that preceded formation of fungal septa. Acto-myosin contractile ring structures are observed at each cell crossing point as the fungus invades rice tissue Bar = 10 μm. **(C)** The polarisome marker Spa2-GFP initially localizes to growing hyphal tips in invasive hyphae (black arrows pointing to the right), but disappear when hyphal tips make contact with host cell wall (white arrows). Spa2-GFP then re-appears at hyphal tips in the adjacent rice cell as it is invaded (black arrows pointing to the left). Bar = 25 μm.

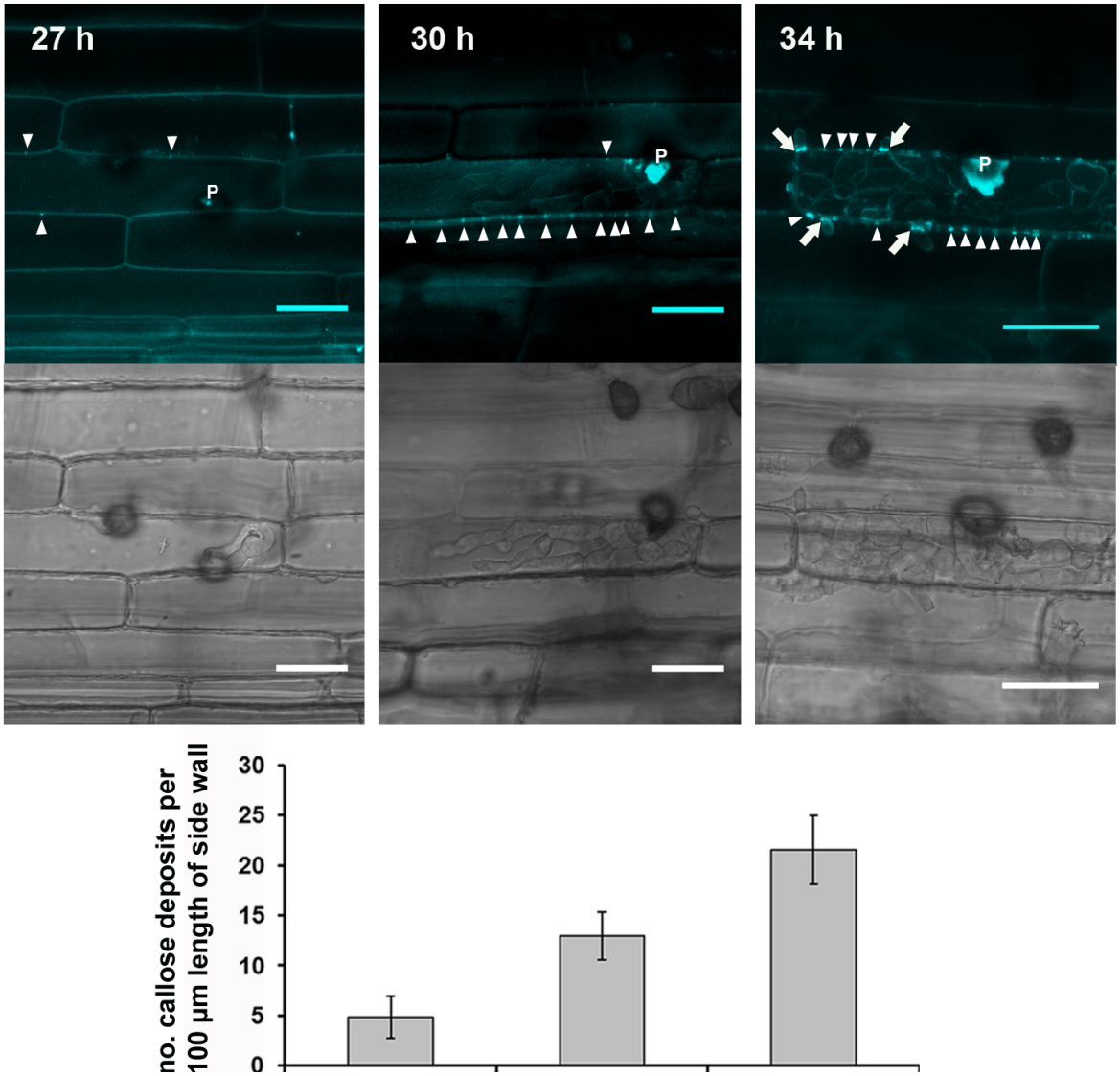

Fig. S3. Dynamics of callose deposits and plasmodesmatal permeability during *M. oryzae* infection. Time course images showing an increase in plasmodesmatal callose deposition in a compatible interaction between *M. oryzae* and rice, over time. Leaf sheaths of CO-39 susceptible rice cultivar were inoculated with the Guy11 wild type strain. Aniline blue staining and laser confocal microscopy were then carried out at 27, 30 and 34 hpi. Three different forms of callose deposition are visible. First, a callose-rich papilla (P) is often visible underneath appressorium penetration sites. Secondly, callose collars form at cell wall crossing sites around invasive hyphae (arrowed). These collars form *after* traversal of the cell wall by *M. oryzae* hyphae in compatible interactions. Finally, callose deposition is observed at plasmodesmata in pit fields (marked by arrow heads). These only become visible once *M. oryzae* has moved beyond the first epidermal cell, consistent with plasmodesmatal closure occurring only after this time, and the loss of viability of initially invaded cells. Bar = 20 µm.

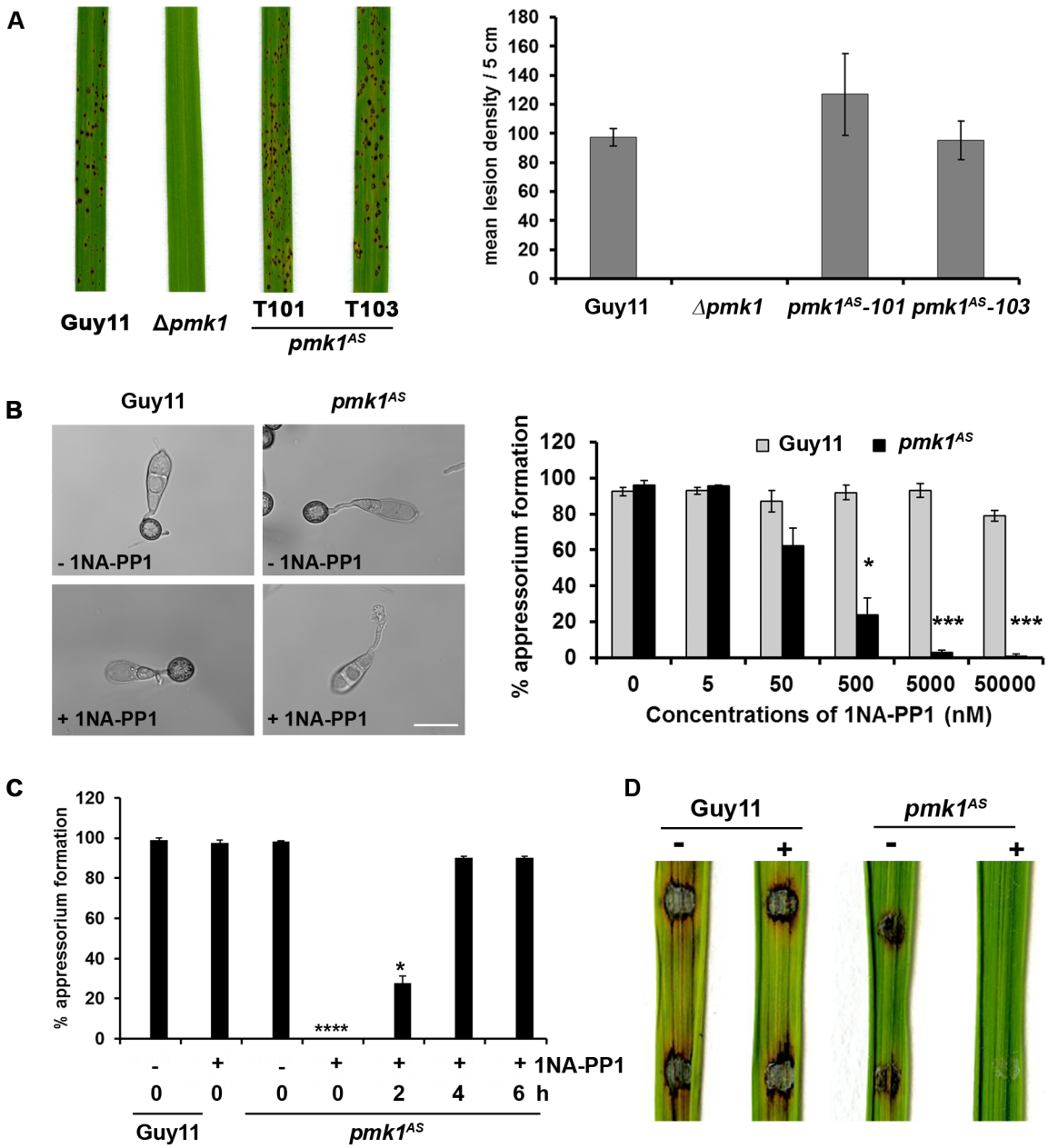

Fig. S4. Introduction the *pmk1*^{AS} allele and selective disruption of *pmk1*^{AS} activity by an ATP analogue. (A) Expression of the *pmk1*^{AS} allele complemented the pathogenicity defects of the Δ*pmk1* mutant (*15*). A suspension of 1 x 10^5 conidia ml^{-1} was sprayed to whole rice plants of cultivar CO-39 (*24*). Lesion density was recorded after 5 days (n = 30 plants). **(B)** Addition of 1NA-PP1 to germinating conidia reduced appressorium formation by the *pmk1*^{AS} strain in a dose-dependent manner, while the Guy11 wild type was not affected. Bar = 20 µm. **(C)** Addition of 5 µM 1NA-PP1 at 4 hours or later did not affect appressorium development. *P < 0.05; ***P < 0.001 (unpaired Student's t test; three biological replicates; 300 spores observed), demonstrating the window of Pmk1 activity necessary for appressorium morphogenesis. **(D)** Leaf drop inoculation assay to show the effect of 1NA-PP1 addition on lesion formation by the *pmk1*^{AS} mutant.

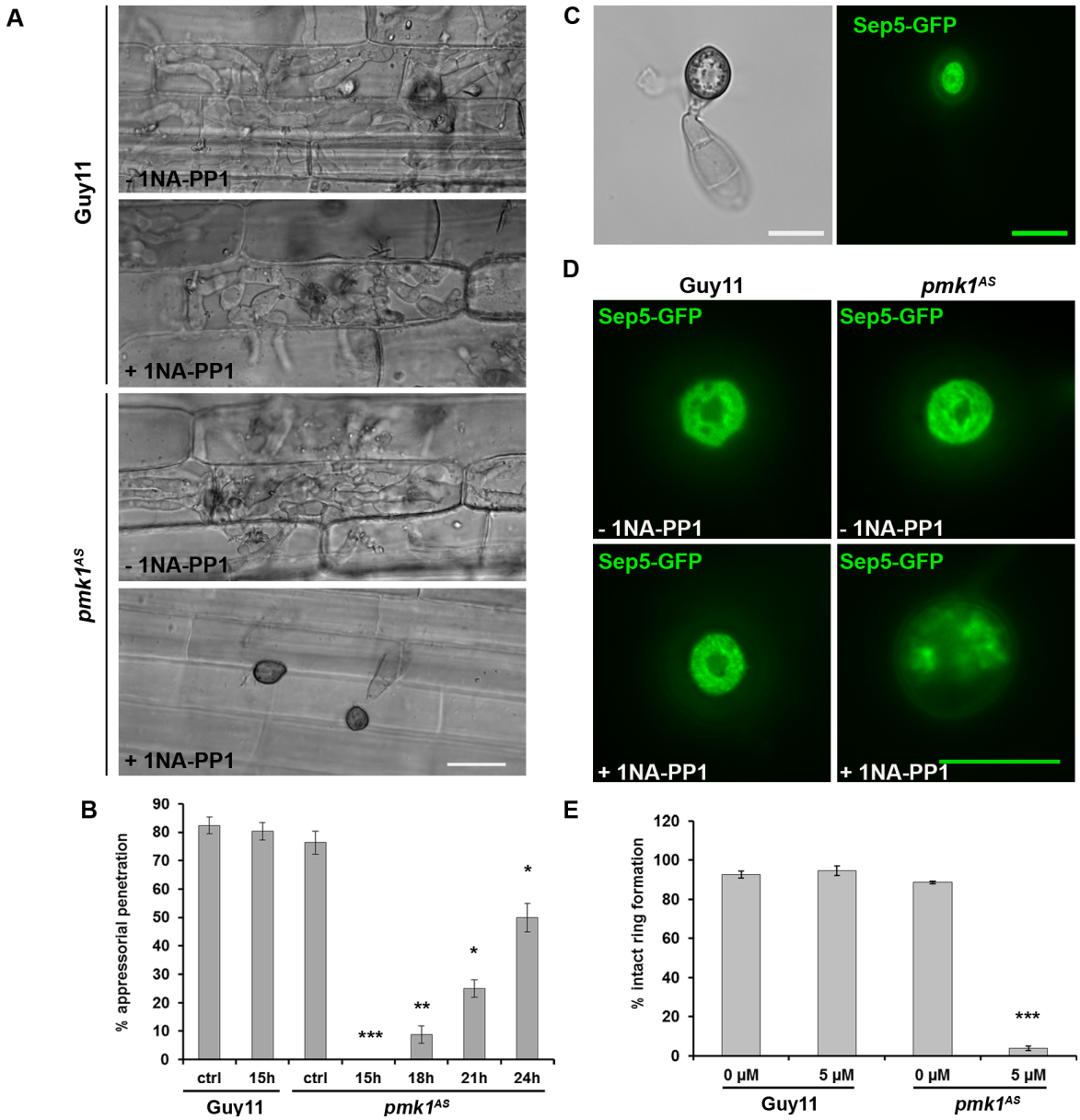

Fig. S5. Pmk1 activity is required for septin-dependent appressorium-mediated cuticle penetration. (A) Micrographs to show the effect of Pmk1 inhibition on appressorium-mediated rice leaf penetration. Appressoria were treated with 5 µM 1NA-PP1 at 15 hpi and infections allowed to proceed until 30 hpi. Bar = 20 µm. **(B)** Bar chart to show the frequency of plant penetration after treatment with 5 µM 1NA-PP1 at different time points. **(C)** Septin ring assembly at the appressorium pore visualized by expression of Sep5-GFP (*3*). **(D)** Inhibition of Pmk1 resulted in mislocalisation of the septin ring in the appressorium pore of *pmk1*^{AS} mutants, resulting in diffused Sep5-GFP accumulation rather than a clear ring-shaped structure. Guy11 or *pmk1*^{AS} appressoria expressing Sep5-GFP developed on cover slips were treated with 5 µM 1NA-PP1 at 6 hours. Bar = 10 µm. **(E)** Bar chart to show the frequency of appressorium showing intact septin rings after appressoria were treated with 1NA-PP1 at 6 hours. **P* < 0.05; ***P* < 0.01; ****P* < 0.001; unpaired Student's *t* test; three biological replicates; 300 spores observed).

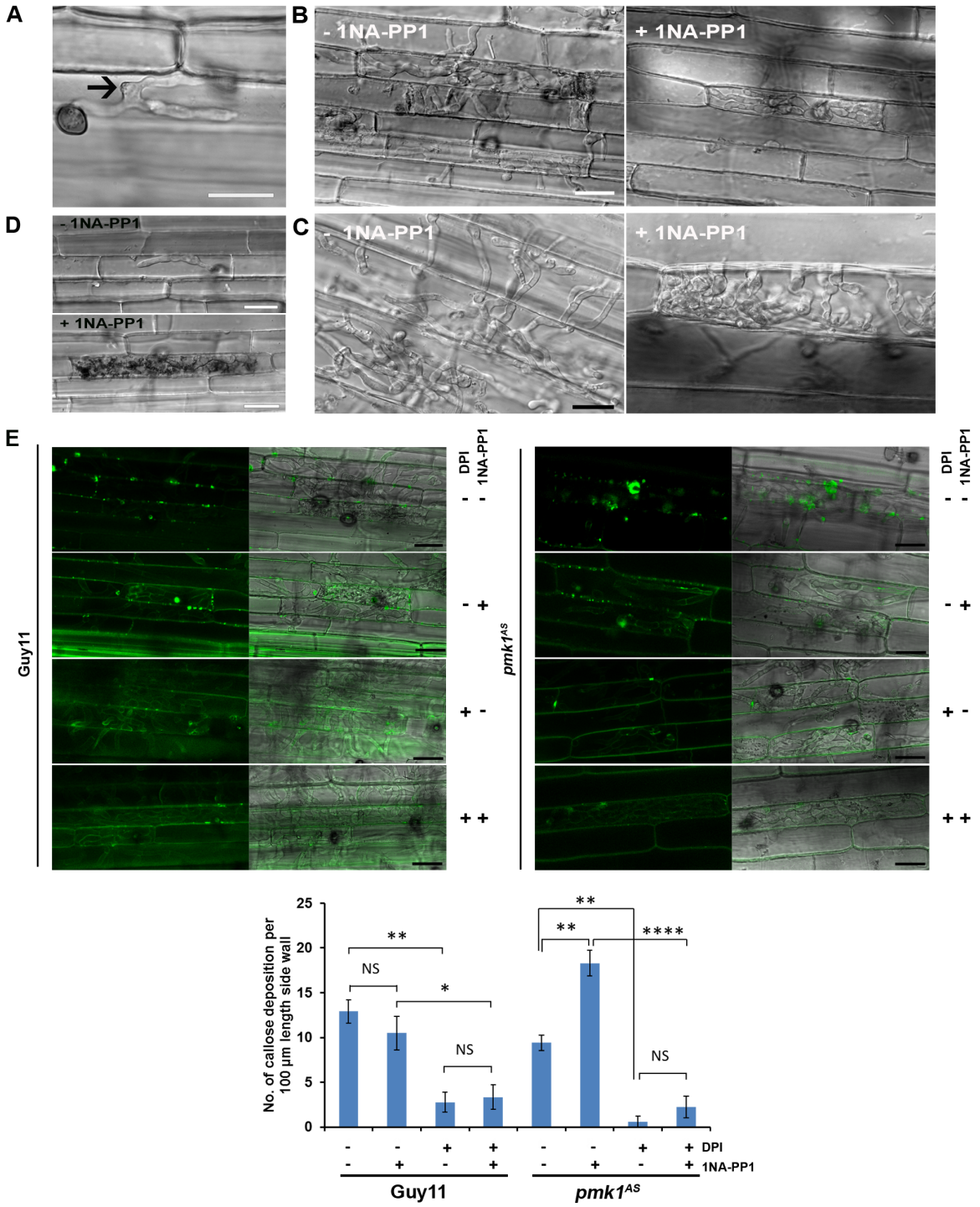

Fig. S6. Chemical genetic inactivation of Pmk1 prevents cell-to-cell invasion of different hosts by *M. oryzae*, and rapidly elicits ROS generation and ROS-dependent callose deposition. (A) Invasive hyphae of the *pmk1*^{AS} mutant at 30 hpi treated with 1NA-PP1 (a 5 µM concentration was added at 26 hpi for all experiments). Arrow indicates a BIC. **(B)** to **(C)** Pmk1 inhibition blocked second cell invasion in the blast-susceptible rice cultivar, Mokoto **(B)** and Golden Promise barley leaf sheaths **(C)**. **(D)** Detection of hydrogen peroxide in infected rice tissue at 30 hpi by DAB staining after addition of 1NA-PP1. **(E)** Representative laser confocal micrographs and quantification of plasmodesmatal callose deposition in rice cells infected with Guy11 or *pmk1*^{AS} strains treated with 1NA-PP1 at 26 hpi in the presence or absence of 0.4 µM DPI, an inhibitor of plant NADPH oxidases, added at 16 hpi, and recorded at 44 hpi. Callose deposition at plasmodesmata is a ROS-dependent process that can be inhibited by DPI. The presence of 1NA-PP1 has no significant effect on Guy11. Addition of 1NA-PP1 to the *pmk1*^{AS} mutant results in a significant increase in ROS-dependent callose deposition at plasmodesmata. This can be prevented by addition of DPI. Callose collars at cell wall crossing points are not ROS-dependent and were visible in Guy11 and untreated samples. They were not counted. *$P < 0.05$; **$P < 0.01$; ****$P < 0.0001$; two-way ANOVA; three biological replicates; n = 30 infected cells. NS, no significant difference. All bars = 20 µm.

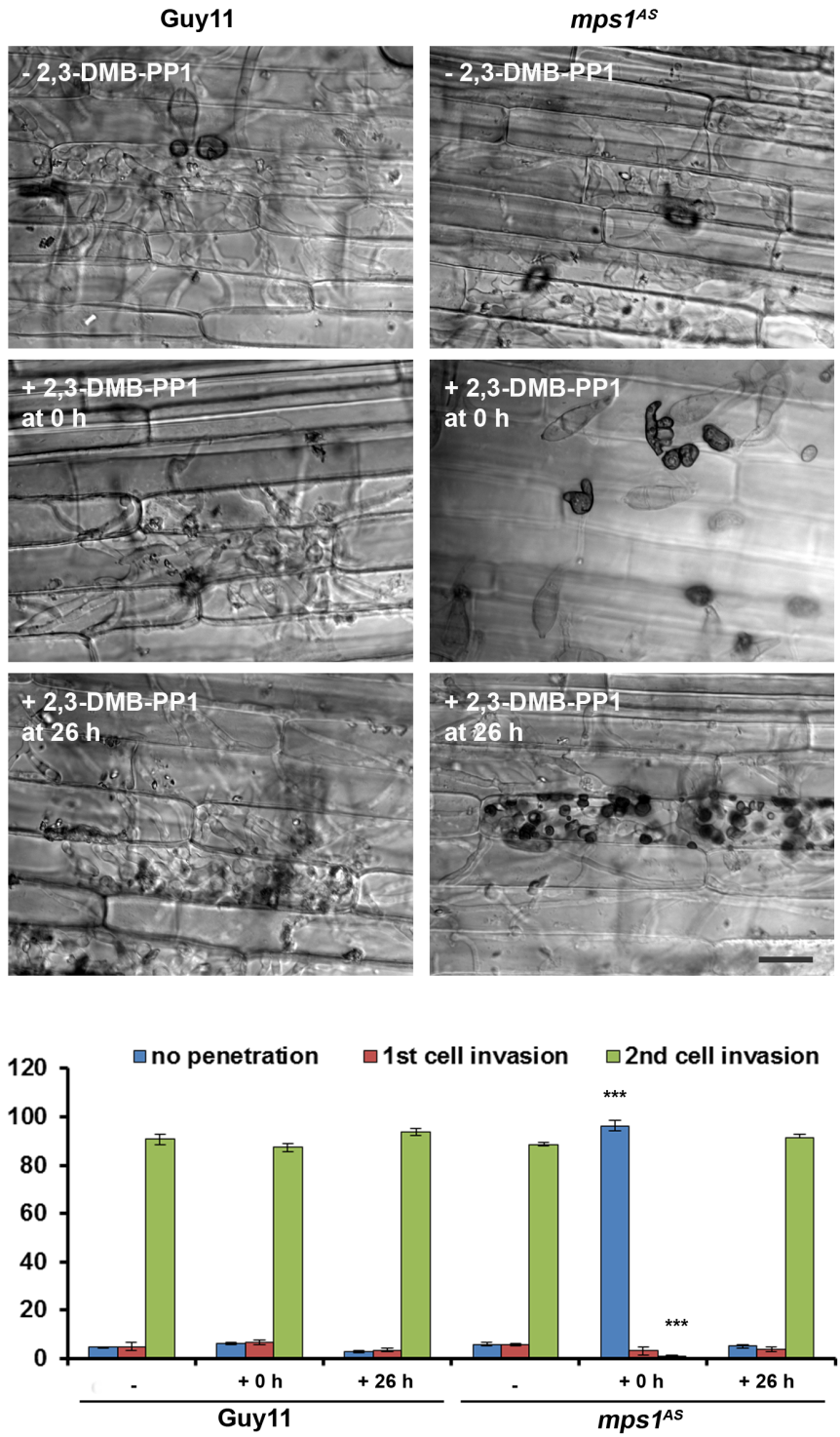

Fig. S7. Inactivation of the cell integrity MAPK Mps1 disrupted appressorium function but did not prevent cell-to-cell invasion in host tissue. The Mps1 MAPK is a functional homologue of yeast Slt2 that is essential for rice blast disease (*18*). We generated a *mps1*^{AS} mutant harboring a E186G mutation based on the previously reported yeast Slt2-as allele (*35*). The *mps1*^{AS} mutant was inoculated on rice leaf sheaths, in the presence or absence of the ATP analogue 4-Amino-1-tert-butyl-3-(2,3-dimethylbenzyl)pyrazolo[3,4-d]pyrimidine (2,3-DMB-PP1) (20 µM) at 0 or 26 hpi, and observed at 48 hpi. Addition of 2,3-DMB-PP1 at 0 h disrupted appressorium morphogenesis and plant penetration by the *mps1*^{AS} mutant, but when the inhibitor was added at 26 hpi the mutant was able to invade neighboring rice cells. Infected rice cells containing *mps1*^{AS} hyphae showed granulation, indicating that the absence of Mps1 activity may elicit, or de-repress, host defense responses (*20*). Bar chart to show frequency of fungal developmental stage. n = 300 infection sites; ***$P < 0.001$; unpaired Student's t test; 300 infection sites observed. Bar = 20 µm.

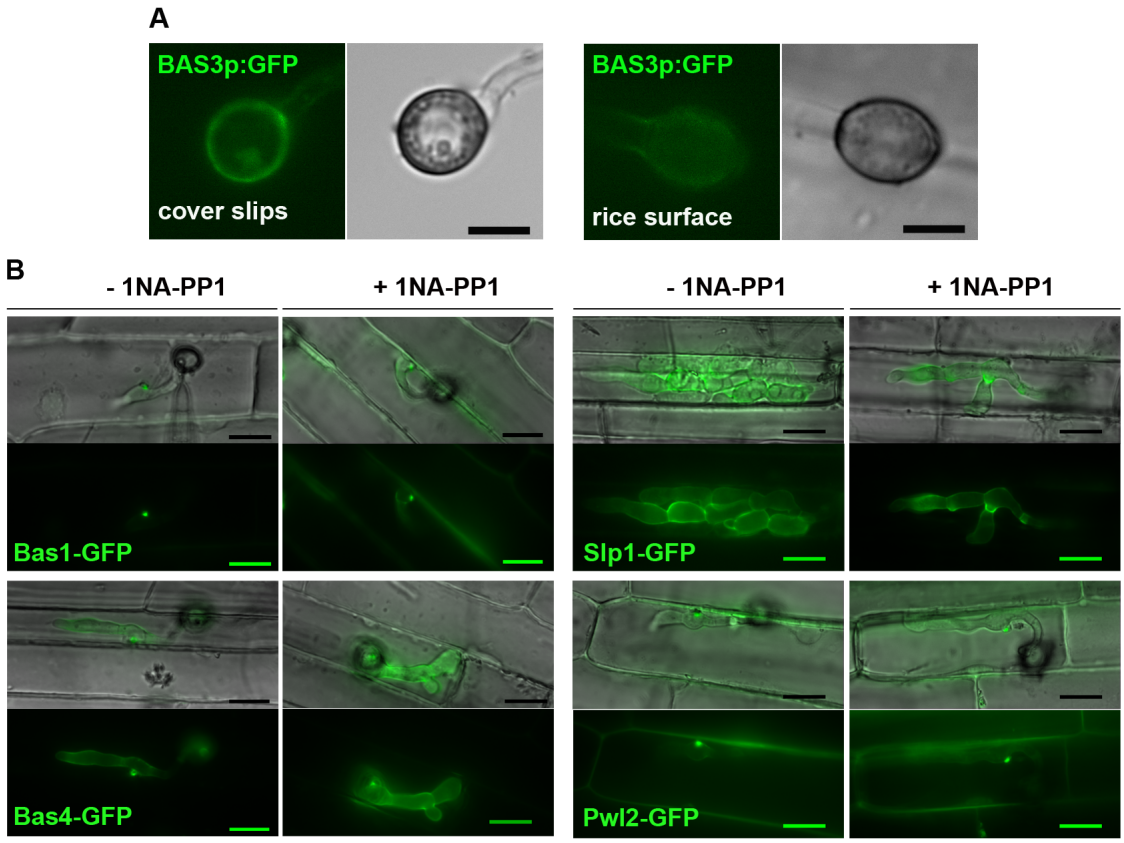

Fig. S8. A sub-set of *M. oryzae* effectors are regulated in a Pmk1-dependent manner during plant infection. (A) Micrographs to show that the *pmk1*^{AS} strain expressing *BAS3p:GFP* did not show GFP fluorescence in appressoria formed on an unyielding artificial surface (left panel), or in an appressorium on a rice leaf surface prior to penetration (right panel), in the absence of 1NA-PP1. Expression was only observed after successful penetration, as shown in Fig. 3D **(B)** Representative epifluorescence micrographs to show localization of Bas1-GFP, Bas4-GFP, Slp1-GFP and PWL2-GFP effector gene fusions in a *pmk1*^{AS} mutant after addition of 1NA-PP1 at 26 hpi. Images were recorded at 32 hours, and selected from of at least 50 infection sites for each experiment. Merged DIC and GFP images are shown in top panels, and GFP signal alone is shown in lower panels. These data demonstrate that not all *M.* oryzae effectors are regulated by Pmk1, but rather that a sub-set of effectors depend on Pmk1 activity for expression during invasive growth. Bar = 20 µm.

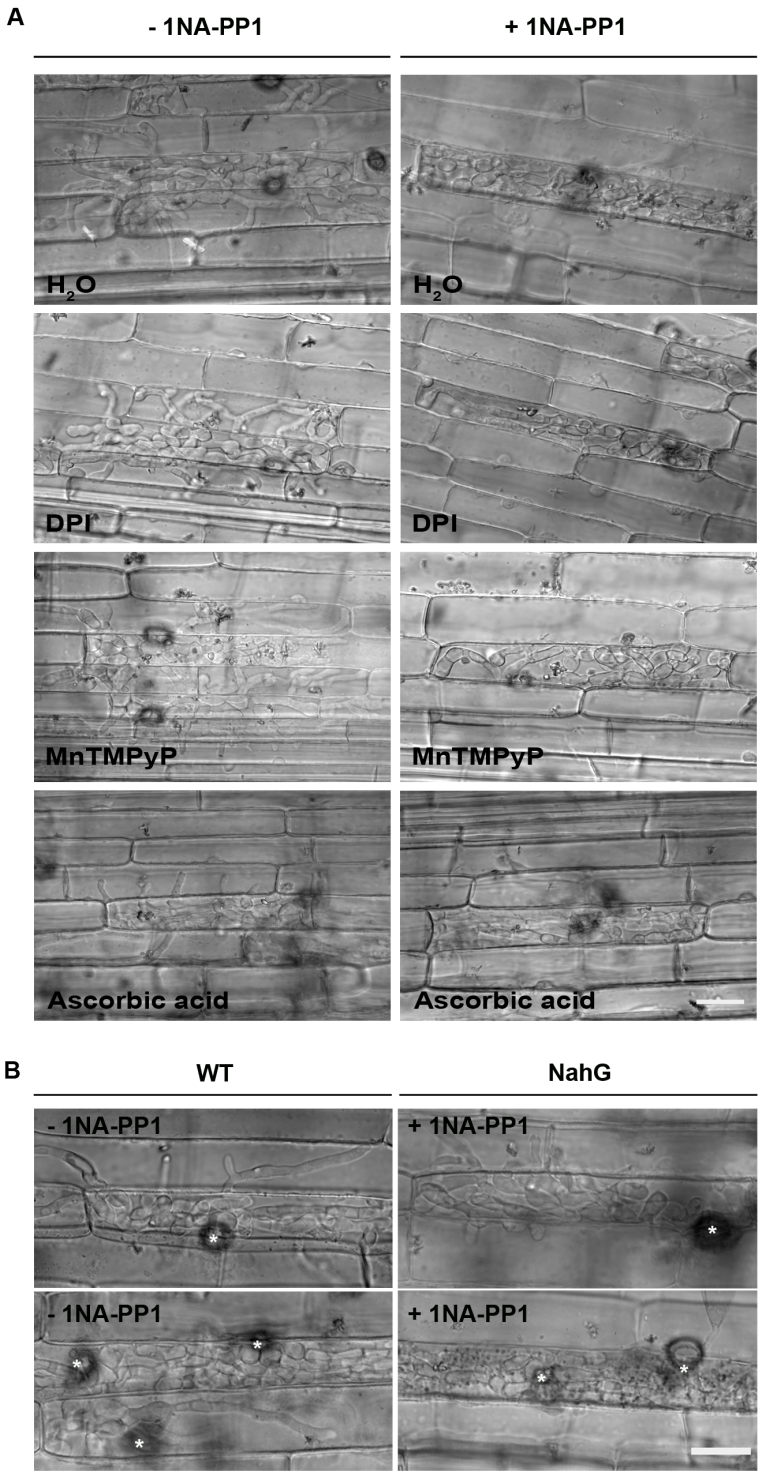

Fig. S9. Inactivation of host defense responses does not rescue the defect in cell-to-cell invasive growth caused by selective inhibition of Pmk1. (A) Representative micrographs showing the effect of ROS inhibition in cell-to-cell movement of the *pmk1*^{AS} mutant. Infected rice sheaths were treated with 10 µM DPI, 100 µM manganese(*35*) tetrakis (1-methyl-4-pyridyl) porphyrin (MnTMPyP), a cell permeable superoxide dismutase mimetic, and the anti-oxidant 10 mM ascorbic acid, in the presence or absence of 5 µM 1NA-PP1 at 26 hpi, and observed at 48 hours. **(B)** Depletion of salicylic acid (SA) did not restore the ability of the *pmk1*^{AS} mutant to cross rice cell walls. Salicylic acid (SA) signaling has been shown to induce plasmodesmatal closure in *Arabidopsis thaliana* (*37*) and depletion of SA levels in rice enhances susceptibility to blast infection (*37*). The SA-deficient NahG transgenic rice line (*37*) and an untransformed wild type (WT) Nipponbare were therefore inoculated with the *pmk1*^{AS} mutant. The ATP analogue 1NA-PP1 (5 µM) was then added to infected rice leaf sheaths at 26 hpi and infection progress assessed at 48 hpi. No second cell invasion was found in 1NA-PP1-treated *pmk1*^{AS} infections of the NahG rice line (n = 100 infection sites for each experiment). Bar = 20 µm .

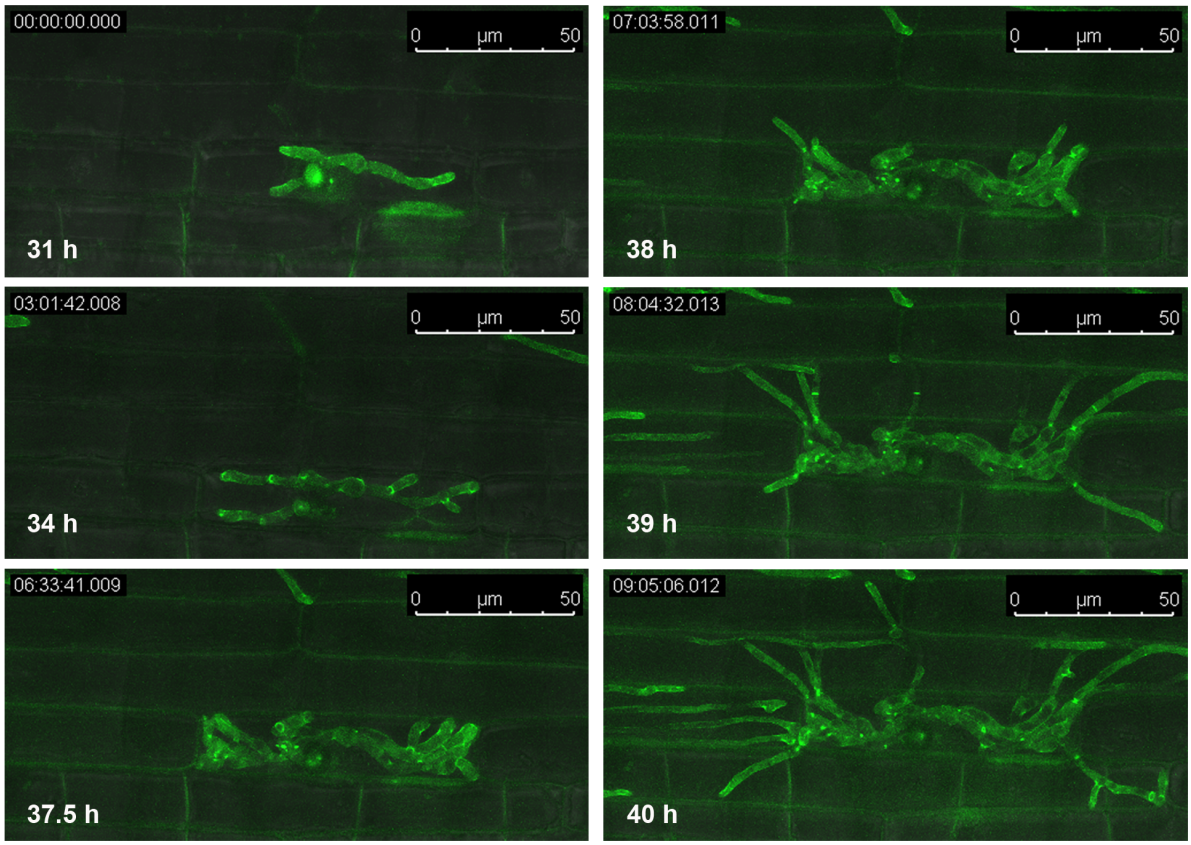

Fig. S10. Time series images extracted from Movie S3 to show invasion of rice tissue and fungal septin dynamics in a *pmk1*^{AS} mutant in the absence of 1NA-PP1. Septin dynamics during rice infection by *M. oryzae* were visualized by laser scanning confocal microscopy of rice leaves infected with a *pmk1*^{AS} mutant expressing Sep5-GFP in the absence of 1NA-PP1 between 3-41 hpi**.** Invasion of adjacent cells can be clearly seen after 38hpi, rapidly moving to colonize rice tissue.

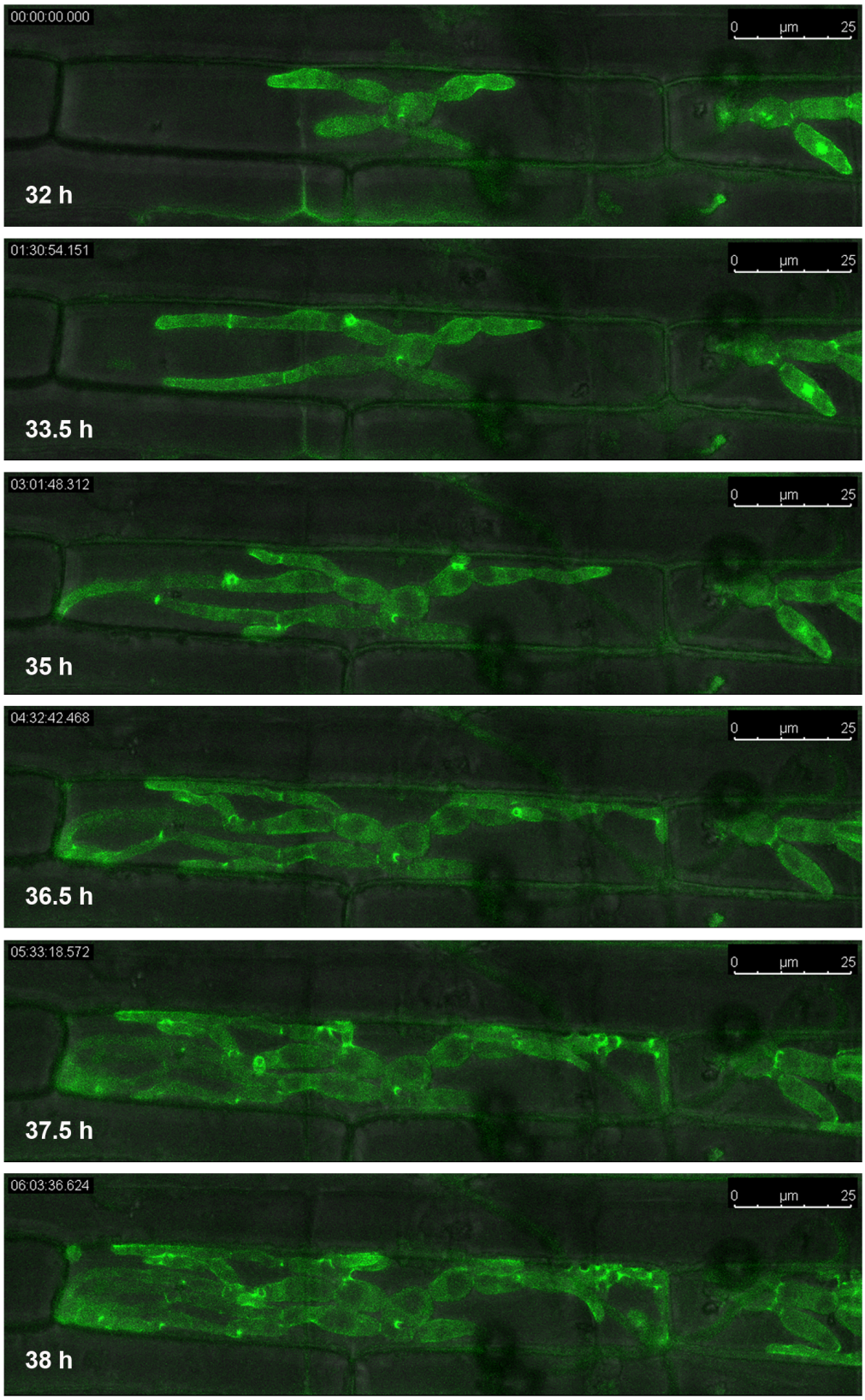

Fig. S11. Time series images extracted from Movie S5 to show entrapment of the *pmk1*^{AS} mutant treated with 1NA-PP1. Rice tissue was inoculated with a *pmk1*^{AS} mutant expressing Sep5-GFP and treated with 1NA-PP1. The mutant was unable to invade beyond the initially invaded rice cell and to send narrow hyphae into adjacent rice cells. The movie was made by visualizing Sep5-GFP localization between 31-37 hpi by laser confocal imaging.

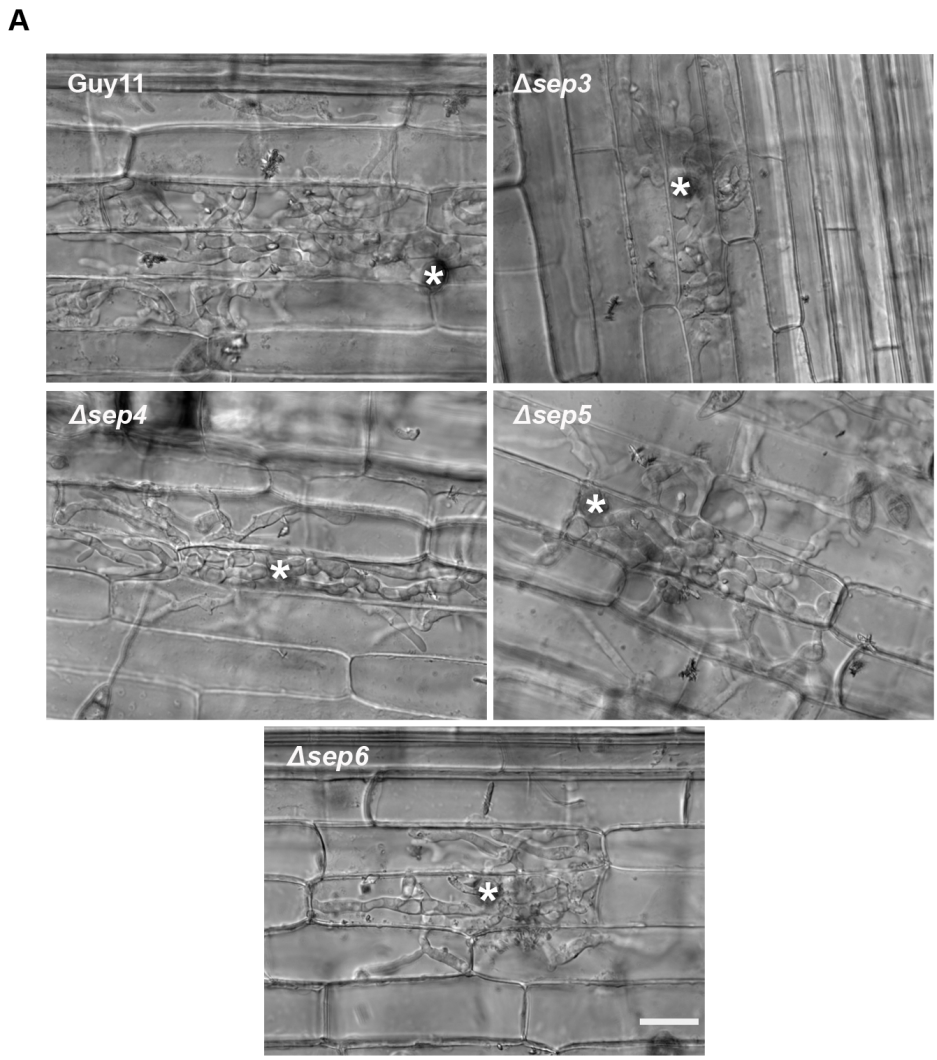

Fig. S12. Fungal septins are involved in cell-to-cell invasion by invasive hyphae of *M. oryzae*. (A) Secondary cell invasion by the wild type strain Guy11 and the isogenic septin mutants, Δ*sep3-6* at 48 hpi (*3*). Asterisks indicate appressorium penetration sites. Bar = 20 µm. **(B)** Bar chart to show frequency of different stages of infection-related development at 48 hours (appressorium without penetration hyphae, first cell invasion and second cell invasion). n = 100 infection sites each experiment; $^{**}P < 0.01$; $^{***}P < 0.001$; unpaired Student's t test, comparing each development stage of each mutant strains with Guy11 wild type. The septin mutants are all impaired in virulence (*3*) and *Δsep3, Δsep5* and *Δsep6* mutants all show severe impairment in appressorium-mediated penetration. Following rare instances of successful appressorium-mediated infection, the *Δsep6* mutant, in particular, shows impairment in cell-to-cell invasion.

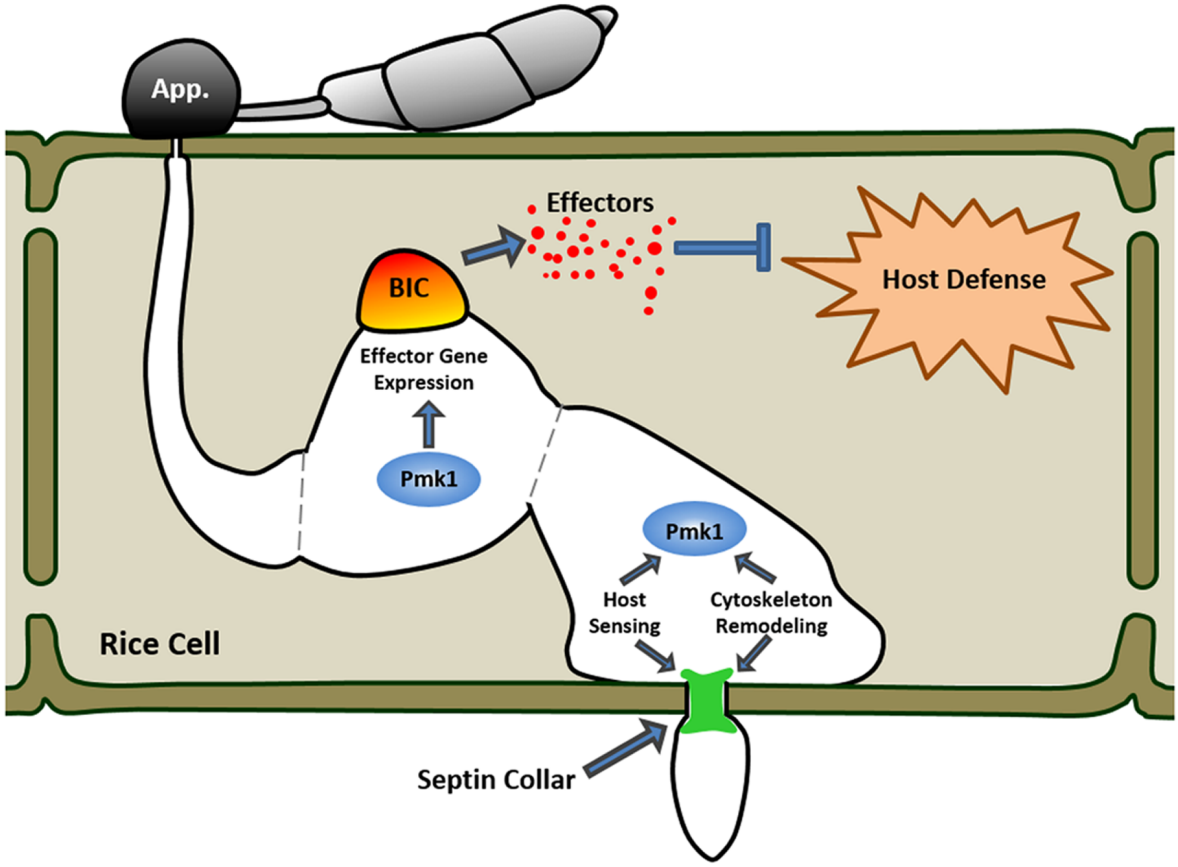

Fig. S13. Model for Pmk1 MAPK-mediated plant cell invasion. The Pmk1 MAPK is a central regulatory of invasive growth by the rice blast fungus *M. oryzae*. The signaling pathway controls the regulation of a sub-set of genes encoding secreted effectors that are involved in host immune suppression, particularly those that act at plasmodesmata. The MAPK pathway also regulates cellular morphogenesis of fungal invasive hyphae which undergo severe constriction as they cross plant cell walls during invasive growth, in order to cause rice blast disease.